Science of the Total Environment 989 (2025) 179850

Contents lists available at ScienceDirect

Science of the Total Environment

journal homepage: www.elsevier.com/locate/scitotenv

Tropical Central African bomb radiocarbon reveals antiphase air-mass atmospheric fluxes and vegetation-growth relationships

Guaciara M. Santos [a,*], Lucas G. Pereira [b], Ana C. Barbosa [b], Santiago Ancapichún [c], Peter van der Sleen [d], Pieter A. Zuidema [d], Peter Groenendijk [e]

[a] Earth System Science Department, University of California, Irvine, USA
[b] Departamento de Ciências Florestais, Universidade Federal de Lavras, Lavras, Brazil
[c] Facultad de Ciencias Forestales y Recursos Naturales, Universidad Austral de Chile, Chile
[d] Department of Environmental Sciences, Wageningen University & Research, Wageningen, Netherlands
[e] Department of Plant Biology, Institute of Biology, University of Campinas, Campinas, Brazil

HIGHLIGHTS

- Radiocarbon (^{14}C) bomb-peak signatures were recorded in an Afrotropical tree.
- Intra-annual ^{14}C of *Entandrophragma utile* tree species shows C-cycle harmonics.
- Maximum to minimum ^{14}C offsets are due to land fluxes and long-range air parcels.
- Northern Hemisphere tree rings provide Austral winter atmospheric ^{14}C information.

GRAPHICAL ABSTRACT

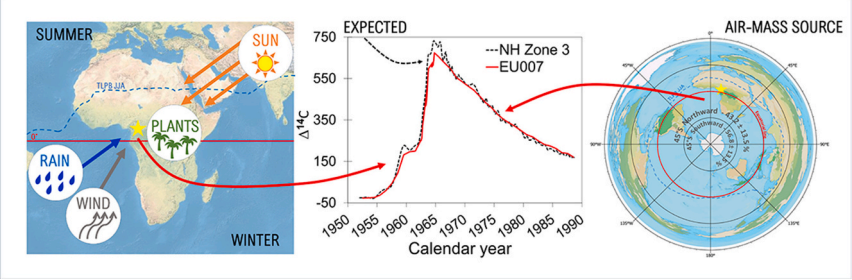

ARTICLE INFO

Editor: Elena Paoletti

Keywords:
Atmospheric ^{14}C reconstruction
Low latitude
Intertropical Convergence Zone
Congo forest
Biotransformation
Land and sea fluxes

ABSTRACT

To achieve more accurate Earth system model projections of diverse climate scenarios, researchers need observation-based data on the movement of carbon between reservoirs, and especially across tropical regions. The Tropical Low-Pressure Belt (TLPB) is a key driver of atmospheric circulation across lower latitudes. While the TLPB shifts across the east–west extent of northern Africa, the extent to which ^{14}C concentrations apply to Afrotropical forests remains untested, restricting our understanding about other carbon feedbacks. Here, we present a high-precision atmospheric ^{14}C record (1940–2012) from a lowland tropical tree species (*Entandrophragma utile*) in Cameroon. We included 107 measurements from whole rings and 15 intra-annual slices. The intra-annual ^{14}C data from 1962, 1963, and 1964 confirm a 7-month long growing season (April–November) with a photosynthetic profile typical of Northern Hemisphere (NH) sites, and showing no nonstructural-carbohydrate interference. The full ^{14}C record reveals that air masses reaching the site were derived primarily from Southern Hemisphere (SH) readings followed by recycled bomb-^{14}C signals from soil and litter. Radiocarbon results were substantiated by HYSPLIT model trajectories coupled with NCEP/NCAR reanalysis data. The paradox of finding that tropical NH trees grow using $^{14}CO_2$ of SH air masses and land-surface respiration

* Corresponding author.
E-mail address: gdossant@uci.edu (G.M. Santos).

https://doi.org/10.1016/j.scitotenv.2025.179850
Received 24 April 2025; Received in revised form 30 May 2025; Accepted 4 June 2025
Available online 12 June 2025
0048-9697/© 2025 The Authors. Published by Elsevier B.V. This is an open access article under the CC BY license (http://creativecommons.org/licenses/by/4.0/).

challenges existing zonal ^{14}C classifications. Our findings highlight an essential role for robust observational ^{14}C data in refining atmospheric models and improving carbon-cycle assessments across distinct climate zones.

1. Introduction

The tropics and their diverse biota offer several essential ecosystem services, including climate regulation, water availability, and food security, impacting both local and global populations (Edwards et al., 2019; Aguirre et al., 2021). Tropical forests are still considered net carbon sinks, due to their capacity to sequester substantial amounts of atmospheric CO_2, as biomass or in their soils (Exbrayat et al., 2017; Hubau et al., 2020; Pan et al., 2024). Different factors, such as geographic location, environmental attributes, species composition, and forest age, can affect forest carbon storage capacity (Poulter et al., 2014; Besnard et al., 2021). The scarcity of spatiotemporal ecological monitoring studies has limited our overall understanding of tropical forest carbon assessments (Wang et al., 2014; Crowther et al., 2015; Villarreal and Vargas, 2021; Pan et al., 2024) and their resilience to the current rate of climate change (Staal et al., 2018; Menne et al., 2012; Zhao et al., 2019; Hubau et al., 2020; Xu et al., 2024). Yet in Tropical Africa, especially the central Congo Basin, studies on tree growth, aboveground biomass and soil carbon stocks remain limited (ForestPlots.net, 2021) compared with those on other topical regions (Groenendijk et al., 2025). Additionally, the Tropical Africa region is influenced by the migration of the Tropical Low-Pressure Belt (TLPB; or the Intertropical Convergence Zone), which is responsible for its seasonal rainfall (Nicholson and Dezfuli, 2013; Longandjo and Rouault, 2024). Besides its potential importance in shaping local climatic conditions, TLPB shifts over Africa import air masses from both continental and tropical ocean sources. Those air masses' contributions are relevant for radiocarbon (^{14}C) analysis, which in turn can help to quantify terrestrial ecosystem carbon cycle processes (Muñoz et al., 2023). Continuous ^{14}C records across lower latitudes are rare (Santos et al., 2024a) or non-existent (Santos et al., 2015, 2020). Establishing a baseline for ^{14}C concentrations across Tropical Africa is a matter of great urgency (Miner et al., 2024), given how climate change is increasingly threatening the tropics (IPCC, 2023).

Radiocarbon dating, used as age assessment of carbonaceous bearing materials, can also be used as an effective carbon tracer (Reimer et al., 2020). Aboveground nuclear bomb testing carried out during the 1950s (Enting, 1982) released considerable amounts of ^{14}C in the atmosphere (Levin and Hesshaimer, 2000), labelling matter as it moved through various carbon pools (Kutschera, 2022). Consequently, tracing the fate of excess bomb ^{14}C in the atmosphere improves understanding of how carbon is stored and turns over in other reservoirs (carbon biogeochemical transformations). Regional atmospheric ^{14}C datasets thus serve as a baseline for understanding air-mass transport or identifying local anthropogenic effects, such as power-plant ^{14}C-releases, biomass and peat burning, and/or fossil fuel emissions (e.g., Varga et al., 2020; Wiggins et al., 2018; Chiquetto et al., 2022). The current global atmospheric post-1950 ^{14}C map employed a geographical division depicted in five distinct zones: three across the Northern Hemisphere (NH1, NH2, and NH3) and two across the Southern Hemisphere (SH1–2 and SH3) (Fig. 1; Hua et al., 2022). This zonal structure of ^{14}C distributions is based on a simple categorization, which groups very short datasets by their latitudinal position. The scarcity of datasets across regions of air-mass confluence, such as the TLPB, has led ^{14}C reconstructions to be poorly represented at lower latitudes. In Tropical Africa, for example, the ^{14}C concentration boundary between NH2 and NH3 (i.e., the TLPB-JJA, where JJA refers to June, July, and August) was determined to be

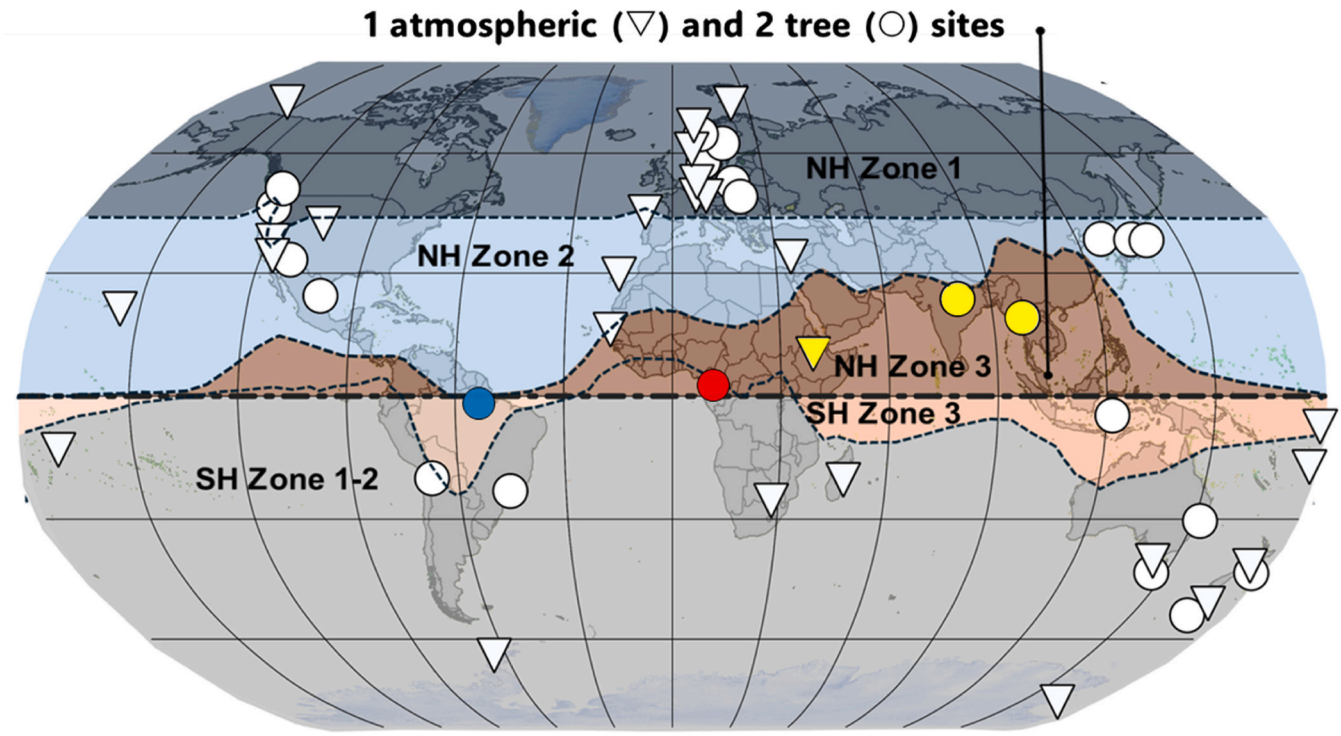

Fig. 1. Global ^{14}C distribution by zones (after Hua et al., 2022), showing sites of atmospheric $^{14}CO_2$ stations (upside-down triangles) and/or tree rings (circles). The NH Zone 3 (or NH3) has been represented by just three short ^{14}C datasets highlighted in yellow, i.e., Debre Zeit, Ethiopia (8°40′N, 38°58′E; 1963–1969; Nydal and Lövseth, 1983), Mandla, India (23°N, 81°E; 1955–1970; Murphy et al., 1997), and Doi Inthanon, Thailand (18°33′N, 98°34′E; 1950–1972; Hua et al., 2000). The blue circle refers to the atmospheric tree ring ^{14}C record of the Eastern Amazon Basin (EAB at 1°S, 53°W; 1940–2016), recently published by Santos et al. (2024a), but not yet part of the global ^{14}C distribution map. The red circle refers to the atmospheric tree-ring ^{14}C Tropical Central African record produced in this study.

near the Sahara Desert, whereas for the NH3 to SH3 (or NH3 to SH1–2) the Equator was designated as the second boundary (TLPB-DJF, where DJF refers to December, January, and February). The poor ^{14}C representation over Tropical Africa is due to two factors, i) the TLPB shifts its position seasonally by a few degrees across this region, and ii) the zone termed NH3 has been portrayed by just three short ^{14}C datasets covering the 1950–1972 period (Fig. 1). When dealing with ^{14}C data gaps—such as those in the NH3 and SH3 zones, which straddle the equatorial line, or fall across regions where jet streams can create boundaries between distinct climatic zones—precipitation patterns caused by TLPB movement from DJF to JJA have been used to infer ^{14}C distributions (Hogg et al., 2020; Hua et al., 2022). From 1973 to 2019, all ^{14}C datasets from NH (i.e., Zones NH1, NH2, and NH3) have been combined into a single compilation (Hua et al., 2022). A similar approach was used to reflect ^{14}C concentrations from 1973 onward in the SH region. Yet significant work is needed to increase representativeness and continuity, especially outside Europe (Fig. 1).

Variations of ^{14}C in the Earth's atmosphere and its carbon-cycle feedbacks require high-resolution data. Worldwide stations sampling atmospheric air-$^{14}CO_2$ are limited (Fig. 1; Hua et al., 2022) and can only be augmented by well-dated tree ring data (Santos et al., 2024a, 2024b; Griffin et al., 2024). However, the misconception that tropical trees did not produce annual rings delayed the development of tropical dendrochronology studies (Worbes, 2002) and atmospheric ^{14}C reconstructions (Reimer et al., 2020) for decades. Many tropical trees produce anatomically distinct annual growth rings (Brienen et al., 2016; Pereira et al., 2018; Granato-Souza et al., 2019) that have been used successfully in ecological, forest management, ecophysiological, and paleoclimatic studies (e.g., Groenendijk et al., 2014; Santos et al., 2015; Hadad et al., 2015; van der Sleen et al., 2015; Baker et al., 2017; Linares et al., 2017; Santos et al., 2020, 2021; Fontana et al., 2024). Robust dendrochronology samples (absolutely dated tree rings) can be used to extend ^{14}C time series, improving understanding of atmospheric dynamics (Santos et al., 2015; Ancapichún et al., 2021), interhemispheric air-mass gradients, and terrestrial carbon fluxes (Santos et al., 2024a), or to infer CO_2 point-source pollution from mining (Santos et al., 2022). Thus, closely aligned dendrochronological and ^{14}C data are paramount to accomplishing high-precision tree-ring based atmospheric ^{14}C measurements (Santos et al., 2024b; Griffin et al., 2024) that are required to help researchers to trace carbon cycle along tropical regions.

In this study, we performed 122 high-precision ^{14}C measurements to produce a complete atmospheric tree ring ^{14}C record from 1940 to 2012 for a well-dated tree-ring sample from Cameroon, Africa (5°N, 9°E). Our main goal was to reconstruct the post-1950 ^{14}C timescale of Tropical Central Africa, a region under a major atmospheric circulation loop, hitherto unexplored. We used intra-annual ^{14}C slices to confirm the

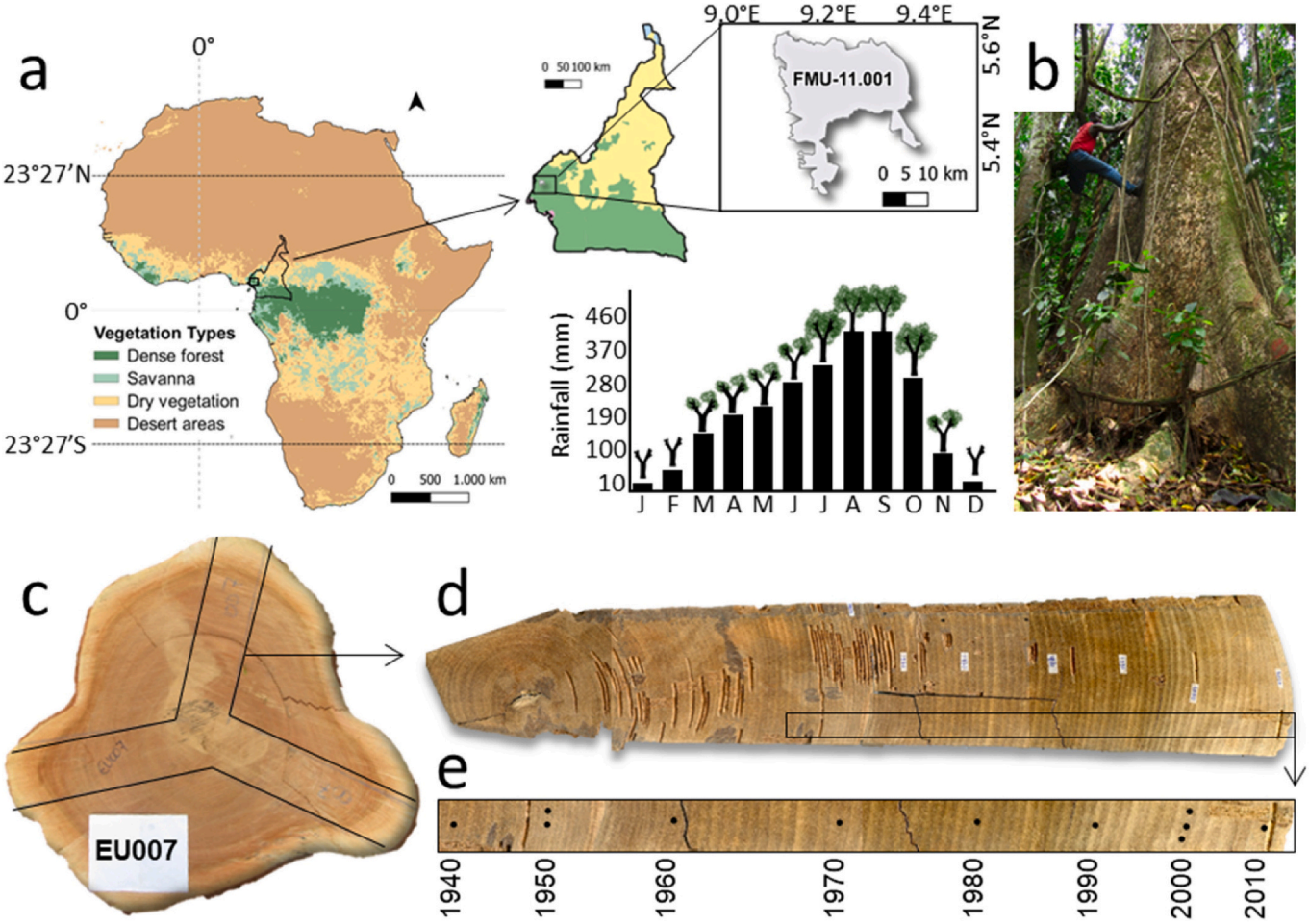

Fig. 2. Tree ring site location characteristics. (a) The *Entandrophragma utile* tree species of Cameroon (5°N, 9°E) was collected at the Forest Management Unit (FMU) 11.001. Regional climate diagram was developed based on data from 1901 to 2022 from the CRU v4.07 database (Harris et al., 2020) and matches with tree species' growth period response to the rainy season (March and November; Poorter et al., 2004). (b) The *E. utile* tree species can grow to a height of 60 m and is considered a tree close to the genus Cedrela in the Neotropics (Yakusu et al., 2018). (c) Cross-section from where the EU007 wood laths (EU007A, EU007B, and EU007C) were removed. (d) Surface of the radial wooden slab (EU007C) showing superficial damage from prescreen isotopic analyses (see Fig. S1 in the Supplementary material). (e) A thin radial cut was used to prepare the subsamples for the ^{14}C reconstruction, with black markings indicating decadal and centennial periods.

growth period of tree species and to investigate nonstructural carbohydrate interference. We discuss our fine-tuned ^{14}C results considering other stand-alone datasets within the NH3 zone (i.e., Debre Zeit, Mandla, and Doi Inthanon; Hua et al., 2022) and from the Eastern Amazon Basin (Santos et al., 2024a). Finally, we used backward trajectory analysis using the HYSPLIT model and the NCEP/NCAR dataset to give insight into the origin of air masses carrying $^{14}CO_2$ to the site, and to infer possible contributions from dry season fires, and land and air-sea sources.

2. Materials and methods

2.1. Sample selection and study area

We obtained our tree sample from the FSC-certified Forest Management Unit 11.001, of Transformation REEF Cameroon (TRC, 2006) in the Southwest Region of Cameroon, located between 5°23′N, 9°09′E and 5°23′N, 9°12′E (Fig. 2). The area lies adjacent to the Korup National Park and about 120 km northeast of the Gulf of Guinea, off the western African coast. The vegetation in the area is characterized as Guineo-Congolian lowland semi-deciduous rainforest (Fig. 2a; Huntley, 2023), which is influenced by the north-south movements of the TLPB. Regional climate is equatorial with a unimodal rainfall precipitation distribution. Total annual rainfall amounts to ~4000 mm (Groenendijk et al., 2014), with a dry season (<100 mm rainfall) lasting from December to February (Fig. 2a). Annual temperature ranges from 23 to 30 °C.

Species of the genus *Entandrophragma* have been shown to produce reliable annual rings (Détienne and Mariaux, 1977) with great potential for dendrochronological studies (Battipaglia et al., 2015). The studied tree species, *E. utile*, is an African mahogany species commercially known as Sipo (Fig. 2b). It is a deciduous species that sheds its leaves during the dry season and restarts growth sometime between March and November in association with the rainy season (Fig. 2c). In some locations, leaf-out may occur as early as February (Poorter et al., 2004). Tree-ring boundaries are delimited by a thin layer of parenchyma that may be preceded by a band of high-density wood tissue, appearing as a distinct dark layer (Figs. 2d,e; Détienne et al., 1998, Groenendijk et al., 2014).

The specimen selected for sampling in this study (shown in Fig. 2d) is part of a collection of 10 individuals spanning approximately 200 years (Groenendijk et al., 2014, 2017). The predominance of complacent rings among the sampled individuals of *E. utile* hindered initial classical dendrochronological analyses. Nonetheless, the annual nature of the species' rings was confirmed by robust correlations between tree-ring $\delta^{18}O$ and annual climatic signals (van der Sleen et al., 2015), and validated by ^{14}C bomb-peak dating of selected calendar years (Groenendijk et al., 2014). Prior to the comprehensive ^{14}C analysis done here, we reconfirmed the yearly ring signatures recorded in the stem disc of *E. utile* (identified as EU007C; Figs. 2d,e) by ^{14}C of another set of 8 calendar years (Fig. S1 and Table S1 – Supplementary material). Retesting of calendar years by ^{14}C was required to ensure that the wood cross section stored for almost a decade was the correct one, and was still under optimal conditions. Neither the ^{14}C results of Groenendijk et al. (2014) nor the prescreen data in Table S1 were included in the subsequent high-accuracy Tropical Central African post-1950 ^{14}C reconstruction produced here, as tree ring cuts in those tests were tentative (Santos et al., 2024b).

After retesting the annual pattern of EU007C, a radial wood slab was sent to the tree-ring laboratory at the Federal University of Lavras (UFLA) where individual rings of the calendar years of interest were carefully singled out using a scalpel. We carefully examined each parenchyma band demarcating ring boundaries and considered the direction of wood tissue growth (Fig. 2e). For the years 1962, 1963, and 1964, we also sampled intra-annual fragments by slicing individual tree rings of each year into five pieces (Fig. S2). This sampling strategy waives the possibility of anchoring the ^{14}C record in time (i.e., within the wet season; Santos et al., 2024a), as those calendar years show the greatest atmospheric ^{14}C shifts once aboveground nuclear tests took place after 1950 (Enting, 1982; Levin and Hesshaimer, 2000).

2.2. Sample handling for isotopic analysis (^{14}C and $\delta^{13}C$)

Labeled micro-vials, each with 7–30 mg of wood, were sent to the University of California, Irvine (UCI) for chemical processing to α-cellulose, graphite production, and high-precision ^{14}C accelerator mass spectrometry (AMS) as well as isotope ratio mass spectrometry (IRMS) analysis. Bulk wood samples were received as single annual and/or intra-annual tree rings. Samples were evaluated under the microscope and reduced to chips with a recovery percentage yield of 99.5 %, following the strategies described in Santos et al. (2024b). To determine tree-ring ^{14}C signatures, we first performed the α-cellulose extraction procedure using acid, alkaline, and bleaching steps (i.e., cycles of 1 N HCl and 1 N NaOH, and 1:1 $NaClO_2$ at 75 °C) followed by 17 % NaOH room temperature and 1 N HCl at 75 °C (Santos et al., 2023). The latter step removes atmospheric-CO_2 absorbed by NaOH, which is crucial for accurate results (Olsson, 1980; Santos et al., 2020). Once homogenized α-cellulose extracts reached pH-neutral by rinses with warm ultra-pure water (18.2 MΩ·cm), they were dried overnight at 60 °C. This straightforward chemical protocol does not use organic solvent and/or acetic acid buffer (Griffin et al., 2024); hence, no carbon-bearing chemicals were ever added during extraction. Individual vials were used for each sample during chemical treatment steps, homogenization and drying procedure, allowing for precise α-cellulose yield calculation (34 %), while avoiding cross-contamination. For ^{14}C data quality control, we used several aliquots of the known-age materials FIRI-J barley (110.7 ± 0.04 pMC; Scott et al., 2004) and AVR-07-PAL-37 ancient wood ($^{14}C > 10$ half-lives; Santos et al., 2023).

About 2 mg of α-cellulose extracts were used to evolve CO_2 by evacuated-sealed quartz tube combustion. Evolved CO_2 was later reduced to filamentous graphite using the Zn method (Santos and Xu, 2017). Graphite targets were measured in a compact in-house modified NEC (0.5MV 1.5SDH-21) spectrometer with $^{13}C/^{12}C$ capabilities, leading to isotopic fractionation correction from biochemical processes and/or spectrometer-induced shifts (Beverly et al., 2010). Radiocarbon results were normalized by 7–8 Oxalic acid I targets (OX-I or NIST HOxI SRM 4990B), the internationally accepted primary standard, using the equations described in Santos et al. (2007). Combustible secondary standards of HOx2 (or NIST HOx2 SRM—4990C) and ANU (sucrose) were also added to each wheel to evaluate spectrometer performance. A total of 73 tree ring samples (1940–2012) were measured in 6 wheels, including 15 intra-annual slices associated with the years of 1962, 1963, and 1964 and many random replicated samples of α-cellulose or wood cuts (122 measurements in total). Radiocarbon abundances of tree rings and intra-annual fractions are presented as decay-corrected $\Delta^{14}C$ values in ‰ units according to Stuiver and Polach (1977), and expressed as $\Delta^{14}C = \{F^{14}C \cdot \exp.[-\lambda(T_i - 1950)] - 1\} \cdot 1000$, where $F^{14}C$ is the normalized ^{14}C concentration to OX-I; λ is the decay constant of $8267y^{-1}$ for ^{14}C; and T_i is the calendar year of wood tissue formation.

Carbon isotopic signatures ($\delta^{13}C$) were derived from α-cellulose remains (~0.7 mg) loaded into 5 × 8 mm tin (Sn) capsules and measured using a continuous-flow FISONS NA 1500 NC Elemental Analyzer connected to a Delta-Plus CF-Isotope Ratio Mass Spectrometer at the KCCAMS/UCI facility. Loaded α-cellulose extracts were measured alongside the reference materials (USGS24 and IAEA-600) and in-house standard (atropine: $C_{17}H_{23}NO_3$). To evaluate if microsite factors affected the isotope composition signatures in tree rings of *E. utile* (Cernusak and Ubierna, 2022), we calculated the tree site $\Delta^{13}C$ values — i.e., the photosynthetic discrimination against ^{13}C — using the equations defined in Farquhar et al. (1989) and the global $\delta^{13}CO_2$ reported in Graven et al. (2017).

2.3. HYSPLIT air parcel trajectory modelling

To forecast the geographic provenances (GP) of $^{14}CO_2$ air parcels that potentially reached Tropical Central Africa (5°N, 9°E) and were assimilated by the *E. utile* tree species, we used backward trajectories by running the Hybrid Single-particle Lagrangian Integrated Trajectory (HYSPLIT) model (Draxler and Hess, 1998; Stein et al., 2015). The HYSPLIT model v.4 was designed to perform a wide range of simulations related to atmospheric transport, including air parcels from local to global scales. For model input, we used the meteorological data found in the NCEP/NCAR (i.e., the National Centers for Environmental Prediction/the National Center for Atmospheric Research) reanalysis dataset (Kalnay et al., 1996), which was derived from satellite and in-situ atmospheric observations. Similar to others (Ancapichún et al., 2021; Santos et al., 2024a), we calculated backward trajectory analysis using only 1 h per day (midday) to determine longitudinal, latitudinal, and altitudinal data points that can trace an air parcel's path back in time (Draxler and Taylor, 1982). Regarding the timeframe, we chose the *E. utile* growing season of April to end of October (7 months in total = 214 days; Fig. 2a) and the years 1949 to 2016.

For ground-level analysis, we used the default altitude of 0.37 km. We then determined the spatial displacement of air parcels during the selected daily time windows — 24 h (1 day) to 120 h (5 days) — into the past. We performed a total of 14,552 backward trajectories over the 7 months modeled (i.e., 214 days × 68 years). To isolate contributions from the NH and SH, we computed air parcels located northward and southward of the TLPB, which here defines the atmospheric circulation boundary between hemispheres. We also evaluated the air-masses contributions from the atmospheric boundary layer (ABL): i.e., the lowest part of the atmosphere, where many physical and chemical mixing processes between the atmosphere and the Earth's surface tend to occur (Garratt, 1994). As a rough approximation, we used 2 km of altitude for the ABL threshold. Of these, we analyzed time windows of every 5 days into the past, from 120 h (5 days) to 600 h (25 days), including variance

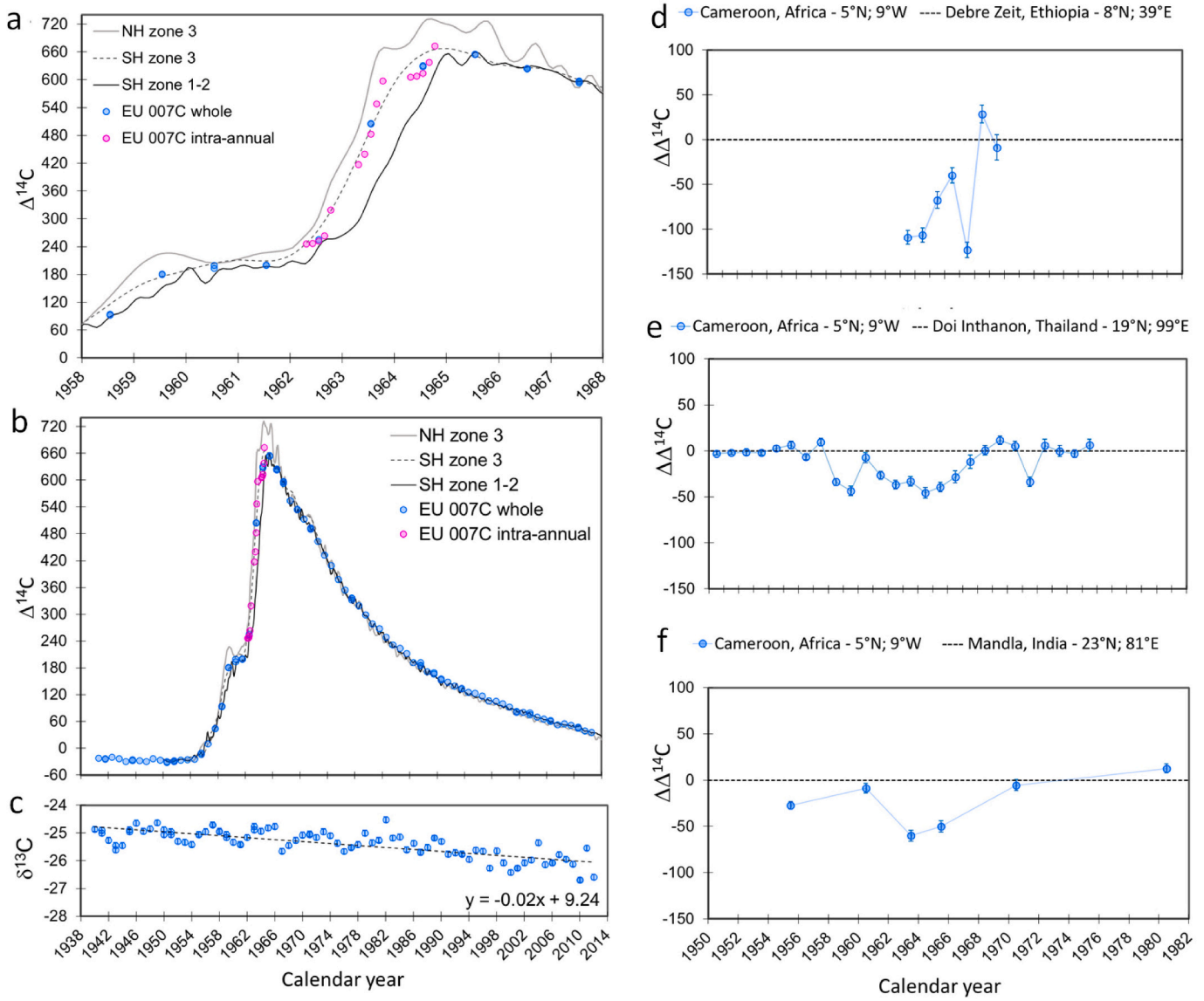

Fig. 3. Variations in carbon isotope values based on tree rings of *E. utile* tree species of Cameroon (5°N, 9°E) are shown as individual $\Delta^{14}C$ values of whole-rings (blue circles) and intra-annual succeeding cuts (pink circles) for: (a) the segment from 1958 to 1968 that comprise the intra-annual ^{14}C data of the 1962, 1963, and 1964; and (b) the complete ^{14}C record (1940–2012). The Hua et al. (2022) NH3, SH3, and SH1-2 curves are also shown. (c) Annual resolution of $\delta^{13}C$-IRMS values is shown for the whole-ring cellulose fibrils. The midpoint of the growing season is 0.541 yrs., this value was added to dendrochronology data (see Fig. S2 for details). Some symbols appear darker due to replicated results. (d, e, f). Residual $\Delta^{14}C$ record was calculated as the difference between the Cameroon ^{14}C fitted values and those of NH3 stand-alone records. Error bars correspond to sum of standard deviation squared of variables subtracted.

from distinct regions. We averaged the hemispheric annual series of air parcel GPs and then divided them by 2.14 (214/100). Thus, 214 is the total number of air parcels modeled by year.

The above-mentioned approach of forecasting the GPs air parcels as ground-level (< 2 km) or ABL analog (≥2 km) allows us to evaluate air masses that: i) originated locally (in the same tropical geographical and climate zone), and ii) are from large regional domains (to estimate conditions of the air masses' transport equilibrium). We also decoupled the upper and lower SH contributions by drawing a line at 45°S (i.e., the 45th parallel south) and calculating the vertical air masses' contributions from those regions.

3. Results

3.1. Cameroonian atmospheric ^{14}C main features based on tree-ring isotopic analysis

Our Cameroonian tree-ring ^{14}C record (1940–2012) was built from 122 measurements (Fig. 3): 15 intra-annual for the years of 1962, 1963, and 1964 (Fig. 3a) and 107 whole rings (Fig. 3b). Annual $\delta^{13}C$ values were also obtained by EA-IRMS (Fig. 3c). Radiocarbon differences (as $\Delta\Delta^{14}C$) between the Cameroonian tree-ring ^{14}C record and the data subsets that build the Hua et al. (2022) NH3 compilation are shown: i.e., the Cameroon $\Delta^{14}C$ values minus Debre Zeit, Doi Inthanon, and Mandla $\Delta^{14}C$ records (Fig. 3d, e, and f, respectively).

Radiocarbon data reproducibility was evaluated by measuring 26 random tree ring pairs/sets (the dark-shaded symbols shown in Fig. 3b, due to overlapping data). A pooled standard deviation yielded <0.2 %, establishing that we achieved a very low statistical variance. This cross-validation also included data pairs of whole rings of calendar years with rapidly increasing ^{14}C signatures, such as 1963 and 1964, determined from distinct wood cuts measured at different timeframes (precision ≤0.15 %). Success in reproducibility and accuracy of ^{14}C data can be attributed to careful sampling of material by the UFLA team, and tree ring handling at KCCAMS lab (99.4 % wood recovery during reduction to particles; Santos et al., 2024b). Sample handling criteria also included microscopy tree-ring cut evaluation, robust chemical treatment, and homogenization of cellulose (Santos et al., 2024b; Griffin et al., 2024). Regarding $\delta^{13}C$-IRMS data, 20 paired data were produced with a precision equal to or better than 0.01 % (Fig. 3c).

For data comparisons in plots (Fig. 3), we considered all ^{14}C zonal compilations of Hua et al. (2022) that are adjacent to Cameroon (i.e., NH3, and SH1-2 and SH3). Taken together, our Cameroon tree-ring ^{14}C record (5°N, 9°E) includes data from the pre-bomb portion (1940–1955) as well as the period of global nuclear bomb testing after 1950 to 2012. Before the bomb pulse rises, our ^{14}C data shows a flat plateau like other ^{14}C records across the tropics (Santos et al., 2024a; Griffin et al., 2024). The typical sharp ^{14}C ascent started after 1954, with a distinctive decline after 1965.

Intra-annual ^{14}C signals based on slices of the years 1962, 1963, and 1964 allowed us to confirm the timing of tissue formation (growing season) and anchored the ^{14}C record at a monthly calendar-year level (Fig. 3a). As growth rings were precisely sliced over discrete increments, we assigned a decimal year to each slice by linking their cuts to time intervals that better reflect wood-tissue growth starting within the wet season (i.e., from April 1 until October 30, when precipitation was >100 mm; Fig. S2). This assumption aligns well with observations by others on African tree species' leaf and cambium responses to precipitation (De Mil et al., 2019), and the common $\delta^{18}O$ signal among *E. utile* tree species with water sources (precipitation and river discharge) and regional climate signals (van der Sleen et al., 2015). Since our intra-annual ^{14}C results from 1962 to 1964 mirror values expected for a single growing season, we can totally dismiss the influence of nonstructural carbohydrate recycling (the readily available sugars and starches; Carbone et al., 2013) biasing stem cellulose, an issue that recently has been observed in studies using extratropical trees (Kromer et al., 2024).

The lack of long-term observational atmospheric data within the TLPB makes it difficult to infer the seasonal cycle of $\Delta^{14}CO_2$ for the tropics. However, the typical two harmonics of the annual seasonal cycle are visible in the Northern Hemisphere atmospheric $\Delta^{14}CO_2$. The carbon cycle harmonics represent the seasonal changes in plant growth (Levin and Kromer, 2004): i.e., photosynthesis (CO_2 absorption during summer) and plant decay (CO_2 release during winter). Our intra-annual Cameroonian ^{14}C values of 1962, 1963, and 1964 growth rings partially display the seasonal cycle harmonics, even though tree growth occurred over only 7 months (Fig. 3a). Cameroon intra-annual partial $\Delta^{14}CO_2$ harmonics are completely in phase with their NH3 compilation analog: i.e., the atmospheric data from Debre Zeit, Ethiopia – 8°N, 38°E (Nydal and Lövseth, 1983), including its amplitude (Fig. S3). Partial $\Delta^{14}CO_2$ harmonics are mostly visible for the summer of 1962 and 1964 (points of deepest drawdown). This consensus confirms the accuracy of decimal dates assigned to intra-annual calendar years (Fig. S2). An increment of 0.541 yrs. was then added to the calendar dates of the whole-year tree-ring dates of *E. utile* running from 1940 to 2012 (Fig. 3) to better reflect its $\Delta^{14}CO_2$ averaged value within the Boreal summer (Fig. S2).

Concerning the bomb peak itself, the maximum observational $\Delta^{14}C$ value detected for Cameroon was 673.3 ± 2 ‰. This $\Delta^{14}C$ value is associated with the fifth intra-annual cut of 1964 (i.e., last fragment of that year, at ca. the beginning of the second week of September; Fig. 3a). In June 1965, we detected a $\Delta^{14}C$ value of 654.7 ± 1.5 ‰ on whole rings (n = 2), a value already lower than that of the previous September (Fig. 3a). Those ^{14}C results contrast with the maximum $\Delta^{14}C$ value reported for the period of June 22–29, 1964, of 781.3 ± 11 ‰ for Debre Zeit (8°N, 38°E; Nydal and Lövseth, 1983), and/or the $\Delta^{14}C$ = 731.6 ± 6 ‰ for the monthly average for mid-August 1964 derived from the NH3 zone curve (Hua et al., 2022). Basically, the Cameroonian bomb-peak $\Delta^{14}C$ maximum value is lower than the mean value(s) associated with the NH3 zone by at least 58 ‰ (Fig. 3b), as well as any other $\Delta^{14}C$ value of the independent 3 datasets that build the NH3 compilation (displayed in Fig. 3d,e,f). Negative values in $\Delta^{14}C$ residuals indicate reversals in the expected NH3 ^{14}C gradient, and as such, they imply differences in air parcel pathways carrying $^{14}CO_2$, and/or the presence of independent carbon sources, such as from fires or fossil emissions, air-sea gas exchange, or land fluxes. Those points have been considered in detail and will be discussed further below.

Regarding anthropogenic fossil fuel emissions over western Africa, Fig. 3c shows a continuous and steady decline in $\delta^{13}C$-IRMS values at our site. We observed a 1.8 ‰ decline between 1940 and 2012, with a dilution rate of approximately 0.017 ‰ per year, based on a simple linear regression that disregarded seasonal variability and the ocean-atmosphere CO_2 exchange. Derived $\Delta^{13}C$ values were then compared to the observed mean values of Cameroonian's precipitation and temperature historical data from 1940 to 2012 (Fig. S4). Although reduced precipitation and increased summer temperatures appear to last from 1985 onward (see Fig. S4), averaged $\Delta^{13}C$ for the latter period (18.30 ± 0.64 ‰; 1985–2012) does not differ significantly from that of the entire period (18.34 ± 0.85 ‰; 1940–2012), denoting that $\delta^{13}C$ drawdown is due to nonpoint-source fossil-fuel contributions (Suess, 1955; Keeling et al., 2001).

3.2. Comparative HYSPLIT backward trajectory analysis during tree growth

Air mass flow to site was evaluated using the HYSPLIT model coupled with NCEP/NCAR reanalysis data within both the ground level (conditions within the same climatic zone) and the upper boundary layer (conditions of air transport from large domains). Fig. 4 depicts a snapshot of the number of air parcels during several specific hours into the past during the growth of the *E. utile* tree species from 1949 to 2016. Globes with density maps show the vertical sum of air parcel contributions in that quadrant for a specific GP (−24, −48, −72, −96, and −120

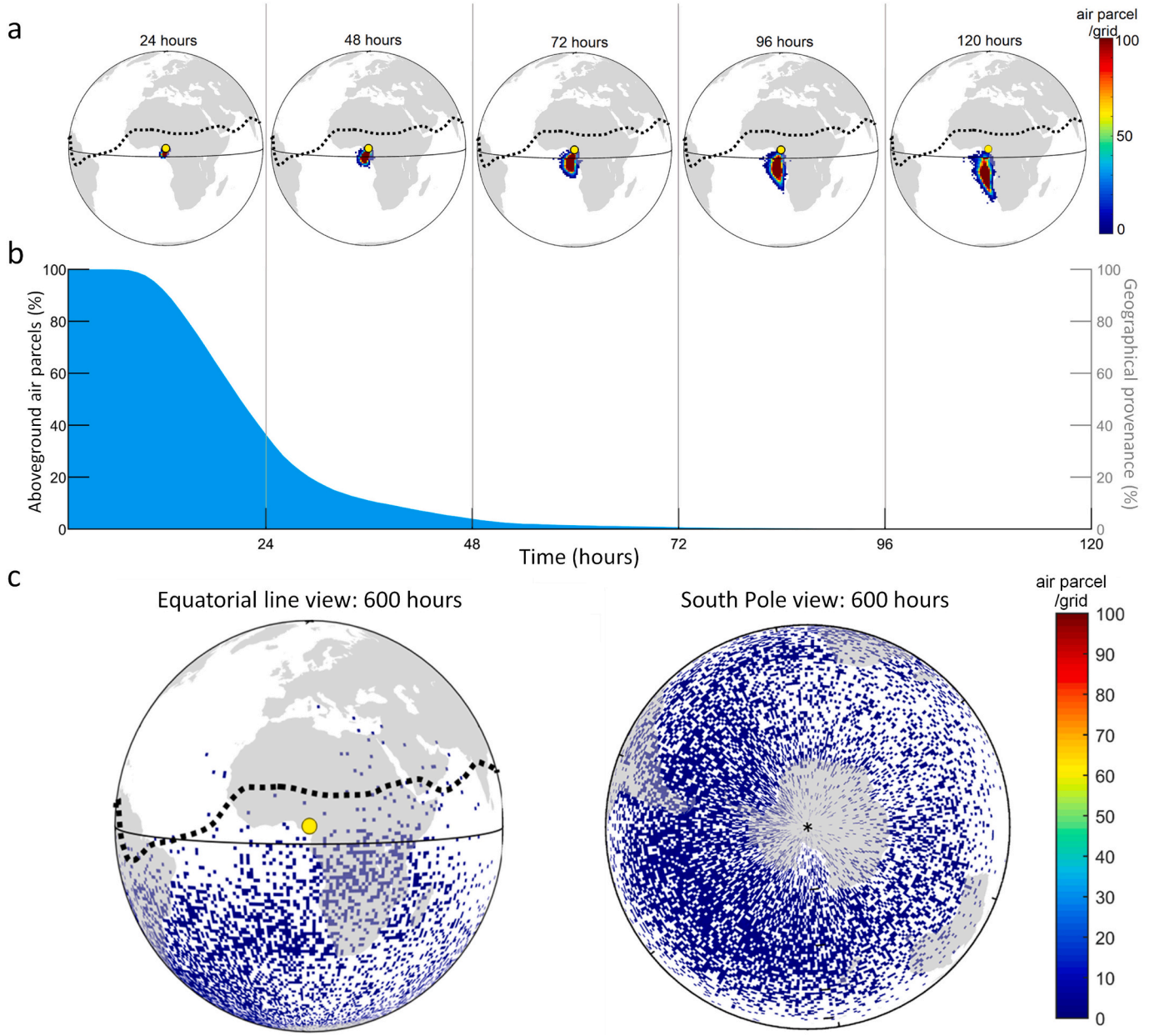

Fig. 4. The HYSPLIT backward trajectory analysis. Density maps for the −24, −48, −72, −96, and −120 h show the vertical sum of air parcel contributions in that quadrant (a), while percentile composite shows aboveground continental versus long-range GP contributions for each time window (b). Full-scale contributions are shown in (c), as 600 h into the past with the focused view on Cameroon (5°N, 9°E) (yellow dot, left), and on South Pole (Antarctic continent, right). The thin black line represents the equatorial line, while the dashed one represents the mean temporal shape of the TLPB during April to the end of October (1949 to 2016). The colored-bar scale (0−100) indicates the density of the GP air parcels. Enlarged images of maps in panel (a) can be found in the supplementary material (Fig. S5).

h; Fig. 4a), while percentage probability contributions offer more precise information on likelihood of air masses: i.e., ground-level versus long-range (Fig. 4b). Finally, Fig. 4c shows contributions from vast GP areas.

Our HYSPLIT – NCEP/NCAR analyses indicates that air masses moving toward Cameroon are indeed from the SH region, with SH defined as southward of TLPB (see Section 2.3). Over 120 h (Fig. 4a), air masses arriving in Cameroon originated from the Atlantic Ocean and follow the shoreline of the African continent until reaching Central Africa's west coast. Thus, emissions from the Congo Basin Forest that straddles the Equator should be considered: e.g., from tropical Cameroon forestlands as well as from the Equatoguinean, Gabonese, and Congolian forests adjacent to the Gulf of Guinea (Fig. 2a). This is relevant, as both land-C fluxes and ocean outgassing may influence our ^{14}C record, with positive or negative offsets, respectively. Air mass regions influencing *E. utile* ^{14}C record can be then specified as: i) generally continental (over 72 h maximum), or ii) mainly oceanic (after 72 h) (Fig. 4b). As time elapsed into the past toward −600 h, we confirmed that air parcel contribution GPs were predominantly molded within the SH region from across sizeable areas, including all continental regions (Fig. 4c and Table 1). Table 1 summarizes the percentage contributions to site of NH, SH, and ABL parameters, beginning at −120 h (with air parcels still over the Gulf of Guinea) and concluding at −600 h (Fig. 4).

It is not in the scope of this article to discuss the mechanisms involved in the global atmospheric circulation process that allow some of the SH mid- and high-latitude air masses to be transferred into the West African region (details in Thorncroft et al., 2011; Nicholson, 2017, 2018; Tamoffo et al., 2024; Longandjo and Rouault, 2024). Nonetheless,

Table 1
Average of air-mass contributions from the Northern Hemisphere (NH), Southern Hemisphere (SH), and the Atmospheric Boundary Layer (ABL; i.e., > 2 km a.s.l.) that arrived at Cameroon during 1949 to 2016 at selected time windows in the past and captured by the *E. utile* tree species. Averages are given in percentage followed by error.

Hours (days) in the past	GP of air-masses (%)		
	NH	SH	ABL
120 (5)	0	100	0
240 (10)	0	89.3 ± 8.2	10.7.2 ± 8.2
360 (15)	0.0 ± 0.1	63.8 ± 13.4	36.2 ± 13.4
480 (20)	0.1 ± 0.2	50.6 ± 10.7	49.3 ± 10.6
600 (25)	0.2 ± 0.4	45.7 ± 9.0	54.2 ± 9.0

to determine the magnitude of the lower SH air masses' contributions to our site, we computed the backward trajectories percentile from south and north of the 45°S line (i.e., the 45th parallel south). We found that 56.8 ± 13.5 % of the air masses are from the upper SH, while 43.2 ± 13.5 % are from higher latitudes, encompassing areas like parts of Patagonia, the southern tip of New Zealand, and Antarctica (Fig. 4c).

4. Discussion

4.1. The seasonal African TLPB excursions and dry-season fires

Along the Atlantic Ocean and over the African continent, the TLPB shifts seasonally following the diagram in Fig. 5, where the combined effects of rainfall and vegetation greenness at the northern sub-Sahara are correlated and in phase with fires further south on the African continent. In short, the TLPB reaches its northmost position at approximately 15°N latitude in August, extending from the westernmost point of Senegal to Ethiopia at the east (Augustin et al., 2023). During this period, southern trade winds carrying oceanic moisture bring heavy rainfall to the northern African region.

In Cameroon, annual rainfall exceeding 100 mm (i.e., from April to November; Dezfuli, 2017) promotes vegetation growth in its deciduous forests (Amraoui et al., 2010; Augustin et al., 2023) (Figs. 2a and 5a). Meanwhile, a contrasting dry season occurs in the SH between the rainforest toward the north (10°S to 15°S) and the Kalahari Desert to the south (Fig. 5a). Biomass burning in savannah-dominated regions tends to occur during this period (Amraoui et al., 2010; Zubkova et al., 2019), and can impact the North African monsoon (Ajoku et al., 2020). The increased smoke, and its ^{14}C isotopic fingerprint, due to SH fires is typically transported into the Gulf of Guinea due to the presence of the southern African easterly jet (Fig. 5a), a central dynamical feature over southern Africa and the southeast Atlantic Ocean. In early fall, the dry northeasterly trade winds from the Sahara start pushing the moist southerly monsoon of western Africa away from land (Cornforth, 2012), promoting dryer conditions that lead to fires (Fig. 5b). The shifted TLPB would then reach its southernmost position in January, south of 5°N (Vondou, 2012), leading to a dry season between the Sahara Desert to the north and the Congo Rainforest to the south (5°N to 15° N) (Fig. 5b).

Fires across the African continent are substantial and occur twice yearly (Fig. 5). Cameroon vegetation may be affected by carbon emissions from such fires during the growth of new wood cells or plant parts (Fig. 4), following the TLPB shifts from JJA to DJF. Based on Adebiyi and Zuidema (2016) determinations, only 8 % of the Central Africa fire plumes leaving the continent to its west between 5°S and 15°S during the dry season would be carried back northwestward (Fig. 5a). Moreover, African fires are dominated by recent vegetation burning (such as tall grasses, savannah/steppes, or croplands that regrow within a year; Fig. 2a), making fire-driven CO_2 emissions to reflect the ^{14}C levels of the same given year. Regarding local biogenic CO_2 contributions, the southeastern region of Cameroon has a low deforestation rate of

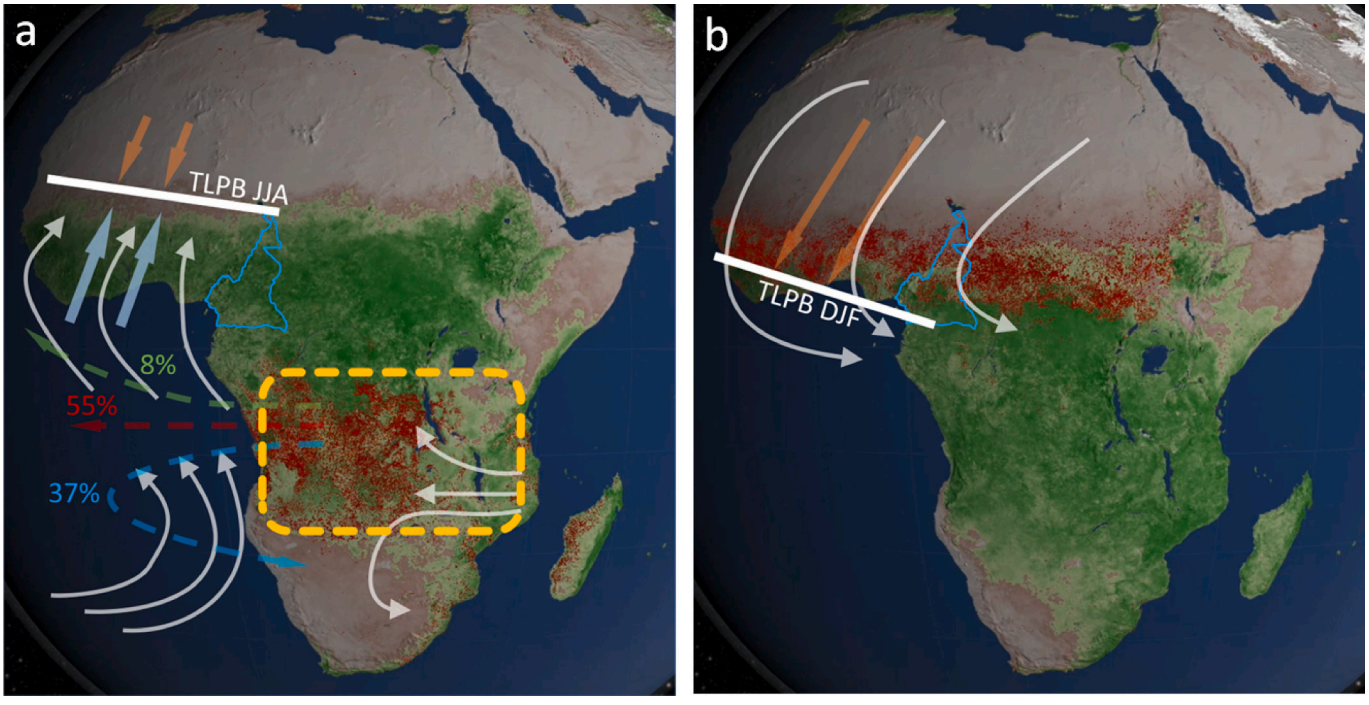

Fig. 5. Seasonal distribution of the winds and fires across Africa during the (a) growing wet season (JJA) and (b) fire dry season (DJF). The contour of Cameroon is shown in light blue, while solid-straight lines indicate the TLPB distinct yearly positions. Main direction of winds flows from the ocean (light blue large arrows) and/or hot land (coral large arrows). Pathways of the fire-driven CO_2 out of the southern Africa region (yellow-dashed box) and their estimated percentages are also shown, as northwestward (green – 8 %), transport westward (red – 55 %), or return to southern Africa (blue – 37 %). Information shown on panels was adapted from multiple works (Adebiyi and Zuidema, 2016; Cornforth, 2012; Dezfuli, 2017; Adebiyi et al., 2023; Augustin et al., 2023). Background images showing seasonal vegetation greenness and burned areas come from NASA/Goddard Space Flight Center (https://www.nasa.gov/goddard/).

approximately 0.07 % per year, while FMU 11.001 recorded 0.02 to 0.03 % (2000–2012, Verhegghen et al., 2016). Local farmers' fires and selective forest management CO_2 contributions during the growing season are also minimal (Tegegne et al., 2016; Verhegghen et al., 2016). Since our radiocarbon data covers the trend of the bomb-peak well on an annual basis (Fig. 3a,b), dry-season or agricultural-fire contributions appear to be irrelevant to the Cameroon ^{14}C record.

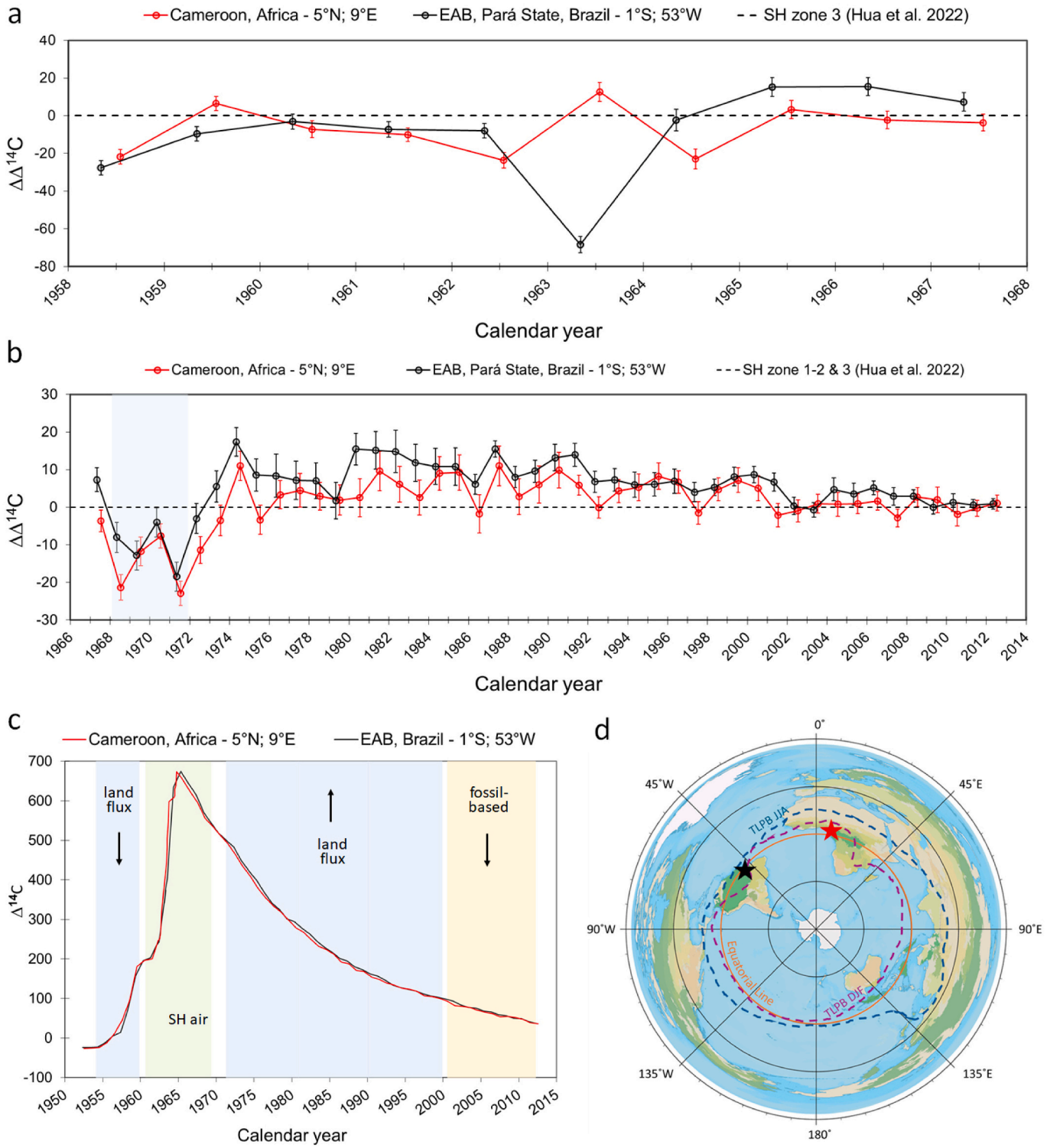

Fig. 6. Residual $\Delta^{14}C$ values calculated as the difference (i.e., $\Delta\Delta^{14}C$) between the Cameroon and EAB tree-ring ^{14}C measured values and fitted curves (SH3; 1958 to 1967 period – Panel a) and (SH1-2 & 3; 1968 to 2012 – Panel b). The latter panel makes use of two compilations to incorporate the fact that SH3 dataset runs from 1950 to 1973 (Hua et al., 2012, 2022). For $\Delta\Delta^{14}C$ calculations (tree-ring ^{14}C record minus Hua et al., 2022 compilation curves), we used the corresponding calendar year period for each record (i.e., 0.541 and 0.340 yrs. for the Cameroon and the EAB ^{14}C records, respectively). Error bars correspond to the sum of standard deviation of the subtracted variables squared. Long-term $\Delta^{14}CO_2$ tree-ring observations are also shown with C sources and drivers indicated (c). The position of each equatorial ^{14}C record and their seasonal TLPB regime, JJA or DJF, is displayed (d).

4.2. Ocean and continental contributions to tropical central African post-1950 ^{14}C record

To better understand atmospheric ^{14}C contributions to the Cameroon site, Fig. 6 presents the trends of $\Delta^{14}CO_2$ differences from the only two complete records near the Equator (Fig. 1), compared to the SH zonal curves of Hua et al. (2022). Those are the ^{14}C Cameroon record under the TLPB (JJA) regime (this study), and the EAB record driven by the TLPB (DJF) (Santos et al., 2024a; Santos et al., 2025). To facilitate comparisons, the data was divided into two sequences: the first covering the period from 1958 to 1967, and the second spanning from 1966 to 2012. We also displayed the complete empiric datasets, the primary air mass source to the site, and the interfering feedback factors that may contribute to ^{14}C-disequilibrium between the atmosphere and biosphere as the TLPB shifts (illustrated on map).

Upwelling along the tropical Atlantic Ocean's margins can add air-sea $^{14}CO_2$ with pre-bomb-pulse levels (negative $\Delta^{14}C$ values) into the atmosphere (Toggweiler et al., 2019). The Benguela upwelling system located off the coast of Namibia (26° to 29°S), facing the Atlantic Ocean, peaks between November and March (Bordbar et al., 2021), and is believed to be involved in the Western African Moonsoon's early phases (Tamoffo et al., 2024). Thus, air-sea degassing to our study site should not be ruled out (Figs. 2a and 4). However, based on our HYSPLIT-NCEP/NCAR analysis data, air masses from subtropical oceans as well as those from ABL are all from long-range transport contributions (Table 1 and Fig. 4). While these large-scale GPs are relevant to Cameroon, they have not depleted (or drawdown) our ^{14}C data. Indeed, Frischknecht et al. (2022) estimated insignificant air-sea degassing transfer at equatorial Africa during the bomb period.

Similarly, urban CO_2 emissions within the African continent do not seem to have a direct effect either (Fig. 6). Fossil fuel emissions with $\Delta^{14}C = -1000$ ‰ can dilute atmospheric $^{14}CO_2$ locally. Cameroon is arguably one of the countries with the lowest emission rates, with just 6.0 $MtCO_2$ per capita during 2017 (Ayompe et al., 2021). This assessment aligns with the ^{14}C data from 2000 onward (Fig. 6b) and findings from $\delta^{13}C$ dilution already shown in Fig. 3c. The agreement between the TLPB atmospheric ^{14}C records (Cameroon and the EAB) and the SH1-2 compilation from 2000 onward (Fig. 6b) supports the notion that overall fossil fuel emissions from the Global South are significantly lower than those from sites further north, which are more strongly influenced by NH regions (Graven et al., 2017; IPCC, 2023).

Radiocarbon differences between 1968 and 1970 (shaded area in Fig. 6b), are due to the absence of the enriched ^{14}C signatures from the aboveground Lop Nur nuclear tests conducted at Xinjiang site, China (42.4°N, 88.3°E; 1964–1980). Its ^{14}C-enriched levels were detected at sites in the Eastern Hemisphere (Hua et al., 2022), but not in South America (Santos et al., 2022, 2024a, 2024b). Lop Nur nuclear detonations were 3–4Mt in magnitude (Enting, 1982), and their contributions may have been confined to the Indo-Pacific region. The $\Delta^{14}C$ differences among sites within the TLPB reinforce the Santos et al. (2024a) hypothesis that amplitude fluctuations in maximum–minimum ^{14}C values exist across this region, contradicting the initial assumption that ^{14}C radioactive dispersion in this climatic zone was relatively uniform.

Fig. 6 also shows atmospheric $\Delta^{14}C$ offsets in Cameroon, i.e., an approximately 20 ‰ depletion in 1958 during the early rise of the bomb pulse and about 10 ‰ enrichment between 1974 and 2000 during its late decline. We hypothesize that those $\Delta^{14}C$ offsets are due to near-surface soil organic carbon (SOC) degassing. This is consistent with what is known as the land-C feedback, predicted by modelling (Randerson et al., 2002 and/or Levin et al., 2022) and demonstrated by Santos et al. (2024a). Aboveground thermonuclear weapon tests have altered SOC $\Delta^{14}C$ values, as well as the fraction released as CO_2 through respiration (Shi et al., 2020). Since respired soil-CO_2 fluxes are governed by soil composition, depth, moisture, temperature, nutrients, and microbe abundances (He et al., 2024), their intensity is biome-driven. Zhao et al. (2024) determined that tropical lands release 58 % of soil-CO_2 compared to temperate and boreal forests (26 % and 16 %, respectively). Gaudinski et al. (2000) demonstrated that soils with $\Delta^{14}C$ values >100 ‰ must contribute significantly to the total soil CO_2 flux. Tchiofo-Lontsi et al. (2020) reported 17.0–18.3 Mg C ha-1 yr-1 of CO_2 fluxes for a lowland rainforest in Cameroon, while Chiti et al. (2010, 2018) reported high $\Delta^{14}C$ values on top SOC layers (≥ 100 ‰) across northwest and Tropical Central Africa. Considering that 100 % of the prevailing air masses close to the Cameroon site are from nearby GPs forested lands (Figs. 4 and S5), Cameroon $\Delta^{14}C$ offset from SH1–2 must be due to soil-CO_2 isoflux reversals (Gaudinski et al., 2000).

To verify the above hypothesis, we took advantage of SOC $\Delta^{14}C$ values reported by Chiti et al. (2010) for south-western Ghana (about 1300 km away from our site) and run a numerical model for mean turnover times (MRT) based on a single/steady C pool reservoir (Fig. S6). We determined that the MRT of carbon in top layers is rather short, i.e., just 5 years for the organic layer (0 - 3 cm) and 10 years for the subsoil (3–45 cm). These shorter MRTs values suggest a higher rate of soil-CO_2 isoflux under Afrotropical forested lands, which when coupled with enriched ^{14}C values (Fig. S6) and air-masses GPs location data at early intervals (Fig. 4), justify the atmospheric ^{14}C enrichment detected at Cameroon ^{14}C record from about 1974 onward (Fig. 6b,c). On the other hand, the Cameroon ^{14}C record's low values in 1958 can be then explained by respired soil-CO_2 negative $\Delta^{14}C$ values (Fig. 6a,c), when tropical surface soil horizons were still dominated by pre-bomb ages (Fig. S6). A similar effect was observed in 1958 at the EAB ^{14}C record as well.

The positive effect of soil-respired CO_2 appears to be, on average, about 2 ‰ lower at the Cameroon site compared to the EAB (Fig. 6b, for example). Cause-effect relationships may also involve inter-hemispheric air mass differences coupled with timing of $^{14}CO_2$ fixation and/or forest size C-absorption and releasing capacity. Air masses arriving at the EAB site happen during austral summer, with 70 % NH contributions carrying higher ^{14}C levels than those from SH (due to the NH-SH ^{14}C time lag; Santos et al., 2024a). Since the Cameroon site receives 100 % of its air from SH at a slightly later time—i.e., during boreal summer— this site is expected to yield somewhat lower $\Delta^{14}C$ values than the EAB. Still, our comprehensive ^{14}C record coupled with air parcel modelling indicated that only a short time period was needed to register the effects of land-atmosphere carbon exchange (Fig. 4). Soil-respired CO_2 with either negative or positive ^{14}C levels was clearly detected in both tropical records discussed here (Fig. 6a,b). This finding aligns with the work of others who reported fast carbon release by different land-C pools in the Amazon Forest (Chanca et al., 2025). Since relationships between %C-concentrations (Shi et al., 2020) and ^{14}C levels of distinct forested soils are still emerging (Chiti et al., 2010, 2018; Drake et al., 2019) and are based on data that are spatially and temporally limited (Chanca et al., 2025, for example), the precise magnitude of forested land-C contributions to recently fixed photosynthates would require further investigation.

4.3. Causation and correlation for Cameroonian atmospheric ^{14}C difference from the NH3 zone

The movement of the TLPB across the great Equatorial Afrotropics is known to be concentrated in the NH—i.e., above the equatorial line. Thus, it is understandable that Hua et al. (2022) assigned the Tropical Central African region to the NH3 ^{14}C concentration zone (Fig. 1). Equatorial air-mass transport influencing atmospheric ^{14}C concentrations along the TLPB is complex and goes beyond the maximum rainfall effect on vegetation growth and its $^{14}CO_2$ fixation notion (Figs. 4 and 5). When studying atmospheric CO_2 fertilization on growth rates of Cameroonian trees, Tandoh et al. (2013) have also found low bomb-peak ^{14}C values within their wood tissue. Researchers attributed lower ^{14}C results to the TLPB migration, but further evaluations on this topic seemed unsuitable, as the studied trees lacked annual rings.

Here, we elucidate the Tropical Central African ^{14}C source-site

paradox. While a small portion of the air masses above the Equator are indeed part of the Cameroon ^{14}C record, they are largely from $^{14}CO_2$ returning from forested ecosystems to the atmosphere (Figs. 4a and 6). A second major contributor of $^{14}CO_2$ to the Cameroon record is the long-range transport of natural and anthropogenic transferred carbon from SH land and sea inventories (Figs. 4c and 6). The NH-SH antiphase shown here, where a tropical tree growing during the NH boreal summer utilizes $^{14}CO_2$ signatures belonging to the SH, illuminates atmospheric ^{14}C concentrations across the TLPB. In addition, the synchronization between the Cameroon ^{14}C record and that of the EAB (associated with the austral summer) would enable the development of an age calibration model specifically for the western hemisphere sector of the TLPB. This is of paramount importance for $\Delta^{14}C$ concentrations in TLPB sites (Santos et al., 2024a), as equatorial atmospheric ^{14}C fluctuations have been modeled (Randerson et al., 2002; Naegler and Levin, 2009; Graven et al., 2017, 2024) despite the lack of observational data.

5. Conclusions

Radiocarbon datasets adjacent to the Equator are typically short and limited, strongly hampering estimations of ^{14}C distributions across this narrow band. However, by combining a tree-ring ^{14}C record (1940–2012) from Cameroon with HYSPLIT backward trajectory analyses, we show that although photosynthesis occurs during the boreal summer, the region receives most of its air masses from the SH as well as terrestrial isoflux reversal. Thus, our ^{14}C-dated Northern Hemisphere tree rings provide a measure of austral winter ^{14}C concentrations. This study's findings highlight the complexity of ^{14}C concentrations across tropical climatic zones and reinforce the need for further high-quality and reproducible data worldwide.

CRediT authorship contribution statement

Guaciara M. Santos: Writing – review & editing, Writing – original draft, Visualization, Validation, Project administration, Funding acquisition, Formal analysis, Data curation, Conceptualization. **Lucas G. Pereira:** Writing – review & editing, Visualization, Methodology. **Ana C. Barbosa:** Writing – review & editing, Visualization, Validation, Resources, Methodology. **Santiago Ancapichún:** Writing – review & editing, Writing – original draft, Visualization, Investigation, Formal analysis. **Peter van der Sleen:** Writing – review & editing, Resources, Methodology. **Pieter A. Zuidema:** Writing – review & editing, Resources, Methodology. **Peter Groenendijk:** Writing – review & editing, Writing – original draft, Resources, Methodology, Investigation, Formal analysis.

Declaration of competing interest

The authors declare that they have no known competing financial interests or personal relationships that could have appeared to influence the work reported in this paper.

Acknowledgments

This research was supported by the United States National Science Foundation to GMS (Grant# AGS-1903690). PG acknowledges financial support by the São Paulo Research Foundation, FAPESP Young Researcher Grant (# 2018/01847-0). ACB thanks CNPq (Grant# PQ 313129/2022-3). LGP was supported by FAPEMIG (Grant# APQ-01544-22). GMS thanks the UCI undergraduate students Lucas Duy Nguyen and June Nakachi Griffin for their valuable help. We sincerely thank the anonymous reviewers and editor for their valuable suggestions.

Appendix A. Supplementary data

Supplementary data to this article can be found online at https://doi.org/10.1016/j.scitotenv.2025.179850.

Data availability

The Cameroon tree ring ^{14}C data used in main text for interpreting air-mass sources and terrestrial isoflux reversals will become permanently available on the UC Irvine Dryad repository upon publication. Other supporting datasets used for comparisons are properly cited in text and the reference list, i.e., Hua et al. (2022) and Santos et al. (2024a) and Santos et al. (2025 - [Dataset], Dryad: https://doi.org/10.5061/dryad.xsj3tx9rd). Background images to produce Fig. 5 came from NASA/Goddard Space Flight Center (https://www.nasa.gov/goddard/).

References

Adebiyi, A.A., Zuidema, P., 2016. The role of the southern African easterly jet in modifying the Southeast Atlantic aerosol and cloud environments. Q. J. R. Meteorol. Soc. 142 (697), 1574–1589. https://doi.org/10.1002/qj.2765.

Adebiyi, A.A., Akinsanola, A.A., Ajoku, O.F., 2023. The misrepresentation of the southern African easterly jet in models and its implications for aerosol, clouds, and precipitation distributions. J. Climate 36 (22), 7785–7809. https://doi.org/10.1175/JCLI-D-23-0083.1.

Aguirre, J., Guerrero, E., Campana, Y., 2021. How effective are protected natural areas when roads are present? An analysis of the Peruvian case. Environ. Econ. Policy Stud. 23, 831–859. https://doi.org/10.1007/s10018-021-00304-y.

Ajoku, O., Norris, J.R., Miller, A.J., 2020. Observed monsoon precipitation suppression caused by anomalous interhemispheric aerosol transport. Climate Dynam. 54 (1), 1077–1091. https://doi.org/10.1007/s00382-019-05046-y.

Amraoui, M., DaCamara, C.C., Pereira, J.M.C., 2010. Detection and monitoring of African vegetation fires using MSG-SEVIRI imagery. Remote Sens. Environ. 114 (5), 1038–1052. https://doi.org/10.1016/j.rse.2009.12.019.

Ancapichún, S., De Pol-Holz, R., Christie, D.A., Santos, G.M., Collado-Fabbri, S., Garreaud, R., Lambert, F., Orfanoz-Cheuquelaf, A., Rojas, M., Southon, J., Turnbull, J.C., Creasman, P.P., 2021. Radiocarbon bomb-peak signal in tree-rings from the Tropical Andes register low latitude atmospheric dynamics in the Southern Hemisphere. Sci. Total Environ. 774, 145126. https://doi.org/10.1016/j.scitotenv.2021.145126.

Augustin, D., Pascal, I.M., Jores, T.K., Elisabeth, F.D., Cesar, M.B., Michael, T.F., Roméo-Ledoux, D.T., Marceline, M., Gladys, K.N.F., Firmin, B.A., 2023. Impact assessment of the West African Monsoon on convective precipitations over the far north region of Cameroon. Adv. Space Res. 72 (3), 666–676. https://doi.org/10.1016/j.asr.2022.04.044.

Ayompe, L.M., Davis, S.J., Egoh, B.N., 2021. Trends and drivers of African fossil fuel CO2 emissions 1990–2017. Environ. Res. Lett. 15 (12), 124039. https://doi.org/10.1088/1748-9326/abc64f.

Baker, J.C.A., Santos, G.M., Gloor, M., Brienen, R.J.W, 2017. Does *Cedrela* always form annual rings? Testing ring periodicity across South America using radiocarbon dating. Trees - Struct. Funct. 31 (6), 1999–2009. https://doi.org/10.1007/s00468-017-1604-9.

Battipaglia, G., Zalloni, E., Castaldi, S., Marzaioli, F., Cazzolla-Gatti, R., Lasserre, B., Tognetti, R., Marchetti, M., Valentini, R., 2015. Long tree-ring chronologies provide evidence of recent tree growth decrease in a central African tropical forest. PLoS One 10 (3), e0120962. https://doi.org/10.1371/journal.pone.0120962.

Besnard, S., Koirala, S., Santoro, M., Weber, U., Nelson, J., Gütter, J., Herault, B., Kassi, J., N'Guessan, A., Neigh, C., Poulter, B., 2021. Mapping global forest age from forest inventories, biomass and climate data. Earth System Science Data Discussions 13 (10), 1–22. https://doi.org/10.5194/essd-13-4881-2021.

Beverly, R.K., Beaumont, W., Tauz, D., Ormsby, K.M., von Reden, K.F., Santos, G.M., Southon, J.R., 2010. The keck carbon cycle AMS laboratory, University of California, Irvine: status report. Radiocarbon 52 (2), 301–309. https://doi.org/10.1017/S0033822200045343.

Bordbar, M.H., Mohrholz, V., Schmidt, M., 2021. The relation of wind-driven coastal and offshore upwelling in the Benguela upwelling system. J. Phys. Oceanogr. 51 (10), 3117–3133. https://doi.org/10.1175/JPO-D-20-0297.1.

Brienen, R.J.W., Schöngart, J., Zuidema, P.A., 2016. Tree rings in the Tropics: insights into the ecology and climate sensitivity of tropical trees. Tree Physiol. 6, 439–461. https://doi.org/10.1007/978-3-319-27422-5_20.

Carbone, M.S., Czimczik, C.I., Keenan, T.F., Murakami, P.F., Pederson, N., Schaberg, P.G., Xu, X., Richardson, A.D., 2013. Age, allocation and availability of nonstructural carbon in mature red maple trees. New Phytol. 200 (4), 1145–1155. https://doi.org/10.1111/nph.12448.

Cernusak, L.A., Ubierna, N., 2022. Carbon isotope effects in relation to CO2 assimilation by tree canopies. In: Siegwolf, R.T.W., Brooks, J.R., Roden, J., Saurer, M. (Eds.), Stable Isotopes in Tree Rings. Tree Physiology, 8. Springer, Cham, pp. 291–310. https://doi.org/10.1007/978-3-030-92698-4_9.

Chanca, I., Levin, I., Trumbore, S., Macario, K., Lavric, J., Quesada, C.A., Carioca de Araújo, A., Quaresma Dias Júnior, C., van Asperen, H., Hammer, S., Sierra, C.A., 2025. How long does carbon stay in a near-pristine central Amazon forest? An empirical estimate with radiocarbon. Biogeosciences 22 (2), 455–472. https://doi.org/10.5194/bg-22-455-2025.

Chiquetto, J.B., Leichsenring, A.R., dos Santos, G.M., 2022. Socioeconomic conditions and fossil fuel CO2 in the Metropolitan Area of Rio de Janeiro. Urban Clim. 43, 101176. https://doi.org/10.1016/j.uclim.2022.101176.

Chiti, T., Certini, G., Grieco, E., Valentini, R., 2010. The role of soil in storing carbon in tropical rainforests: the case of Ankasa Park, Ghana. Plant and Soil 331, 453–461. https://doi.org/10.1007/s11104-009-0265-x.

Chiti, T., Rey, A., Jeffery, K., Lauteri, M., Mihindou, V., Malhi, Y., Marzaioli, F., White, L. J., Valentini, R., 2018. Contribution and stability of forest-derived soil organic carbon during woody encroachment in a tropical savanna. A case study in Gabon. Biol. Fertil. Soils 54, 897–907. https://doi.org/10.1007/s00374-018-1313-6.

Cornforth, R., 2012. Overview of the west African monsoon 2011 1. Weather 67 (3), 59–65. https://doi.org/10.1002/wea.1896.

Crowther, T.W., Glick, H.B., Covey, K.R., Bettigole, C., Maynard, D.S., Thomas, S.M., Smith, J.R., Hintler, G., Duguid, M.C., Amatulli, G., Tuanmu, M.N., 2015. Mapping tree density at a global scale. Nature 525 (7568), 201–205. https://doi.org/10.1038/nature14967.

De Mil, T., Hubau, W., Angoboy Ilondea, B., Rocha Vargas, M.A., Boeckx, P., Steppe, K., Van Acker, J., Beeckman, H., Van den Bulcke, J., 2019. Asynchronous leaf and cambial phenology in a tree species of the Congo Basin requires space–time conversion of wood traits. Ann. Bot. 124 (2), 245–253. https://doi.org/10.1093/aob/mcz069.

Détienne, P., Mariaux, A., 1977. Nature et périodicité des cernes dans les bois rouges de Méliacées africaines. Bois & Forets Des Tropiques 175 (175), 52–61. https://doi.org/10.19182/bft1977.175.a19310.

Détienne, P., Oyono, F., Madron, L., Demarquez, B., Nasi, R., 1998. L'analyse de cernes: Applications aux études de croissance de quelques essences en peuplements naturels de forêt dense africaine. Serie FORAFRI No. Document 15. CIRAD-Foret, Montpellier, France 39p.. http://agritrop.cirad.fr/315473/1/ID315473.pdf.

Dezfuli, A., 2017. Climate of western and central equatorial Africa. In: Oxford research encyclopedia of climate science. https://doi.org/10.1093/acrefore/9780190228620.013.511 (Retrieved 10 Apr. 2024, from).

Drake, T.W., Van Oost, K., Barthel, M., Bauters, M., Hoyt, A.M., Podgorski, D.C., Six, J., Boeckx, P., Trumbore, S.E., Cizungu Ntaboba, L., Spencer, R.G., 2019. Mobilization of aged and biolabile soil carbon by tropical deforestation. Nat. Geosci. 12 (7), 541–546. https://doi.org/10.1038/s41561-019-0384-9.

Draxler, R., Hess, G., 1998. An overview of the HYSPLIT_4 modeling system for trajectories, dispersión, and deposition. Austrian Meteorological Magazine 47, 295–308 (ISSN: 0004-9743).

Draxler, R., Taylor, D., 1982. Horizontal dispersion parameters for long-range transport modelling. J. Appl. Meteorol. 21 (3), 367–372. https://doi.org/10.1175/1520-0450(1982)021<0367:HDPFLR>2.0.CO;2.

Edwards, D.P., Socolar, J.B., Mills, S.C., Burivalova, Z., Koh, L.P., Wilcove, D.S., 2019. Conservation of tropical forests in the anthropocene. Curr. Biol. 29 (19), R1008–R1020. https://doi.org/10.1016/j.cub.2019.08.026.

Enting, I.G., 1982. Nuclear Weapons Data for Use in Carbon Cycle Modelling (No. 44). Commonwealth Scientific and Industrial Research Organization (C.S.I.R.O.), Melbourne (Australia), pp. 1–19 (ISBN: 0643034609).

Exbrayat, J.F., Liu, Y.Y., Williams, M., 2017. Impact of deforestation and climate on the Amazon Basin's above-ground biomass during 1993–2012. Sci. Rep. 7 (1), 15615. https://doi.org/10.1038/s41598-017-15788-6.

Farquhar, G.D., Ehleringer, J.R., Hubick, K.T., 1989. Carbon isotope discrimination and photosynthesis. Annu. Rev. Plant. Physiol. Plant. Mol. Biol. 40 (1), 503–537.

Fontana, C., López, L., Santos, G.M., Villalba, R., Hornink, B., Assis-Pereira, G., Roig, F. A., Tomazello-Filho, M., 2024. A new chronology of Cedrela fissilis (Meliaceae) for Southern Brazil: combining classical dendrochronology and radiocarbon dating. Dendrochronologia 85, 126214. https://doi.org/10.1016/j.dendro.2024.126214.

ForestPlots.net, 2021. Taking the pulse of Earth's tropical forests using networks of highly distributed plots. Biol. Conserv. 260, 108849. https://doi.org/10.1016/j.biocon.2020.108849.

Frischknecht, T., Ekici, A., Joos, F., 2022. Radiocarbon in the land and ocean components of the community earth system model. Glob. Biogeochem. Cycles 36 (1), e2021GB007042. https://doi.org/10.1029/2021GB007042.

Garratt, J., 1994. Review: the atmospheric boundary layer. Earth Sci. Rev. 37, 89–134. https://doi.org/10.1016/0012-8252(94)90026-4.

Gaudinski, J.B., Trumbore, S.E., Davidson, E.A., Zheng, S., 2000. Soil carbon cycling in a temperate forest: radiocarbon-based estimates of residence times, sequestration rates and partitioning of fluxes. Biogeochemistry 51, 33–69. https://doi.org/10.1023/A:1006301010014.

Granato-Souza, D., Stahle, D.W., Barbosa, A.C., Feng, S., Torbenson, M.C.A., Pereira, G. A., Schöngart, J., Barbosa, J.P., Griffin, D., 2019. Tree rings and rainfall in the equatorial Amazon. Climate Dynam. 52, 1857–1869. https://doi.org/10.1007/s00382-018-4227-y.

Graven, H., Allison, C.E., Etheridge, D.M., Hammer, S., Keeling, R.F., Levin, I., Meijer, H. A., Rubino, M., Tans, P.P., Trudinger, C.M., Vaughn, B.H., 2017. Compiled records of carbon isotopes in atmospheric CO2 for historical simulations in CMIP6. Geosci. Model Dev. 10 (12), 4405–4417. https://doi.org/10.5194/gmd-10-4405-2017.

Graven, H.D., Warren, H., Gibbs, H.K., Khatiwala, S., Koven, C., Lester, J., Levin, I., Spawn-Lee, S.A., Wieder, W., 2024. Bomb radiocarbon evidence for strong global carbon uptake and turnover in terrestrial vegetation. Science 384 (6702), 1335–1339. https://doi.org/10.1126/science.adl4443.

Griffin, J.N., Santos, G.M., Nguyen, L.D., Rodriguez, D.R.O., Pereira, L.G., Jaén-Barrios, N., Assis-Pereira, G., Barreto, N.O., Brandes, A.F.N., Barbosa, A.C., Groenendijk, P., 2024. Demystifying the tropics: FTIR characterization of pantropical woods and their α-cellulose extracts for past atmospheric 14C reconstructions. Sci. Total Environ. 949, 175010. https://doi.org/10.1016/j.scitotenv.2024.175010.

Groenendijk, P., Sass-Klaassen, U., Bongers, F., Zuidema, P.A., 2014. Potential of tree-ring analysis in a wet tropical forest: a case study on 22 commercial tree species in Central Africa. For. Ecol. Manage. 323, 65–78. https://doi.org/10.1016/j.foreco.2014.03.037.

Groenendijk, P., Bongers, F., Zuidema, P.A., 2017. Using tree-ring data to improve timber-yield projections for African wet tropical forest tree species. For. Ecol. Manage. 400, 396–407. https://doi.org/10.1016/j.foreco.2017.05.054.

Groenendijk, P., Babst, F., Trouet, V., Fan, Z.X., Granato-Souza, D., Locosselli, G.M., Mokria, M., Panthi, S., Pumijumnong, N., Abiyu, A., Acuña-Soto, R., 2025. The importance of tropical tree-ring chronologies for global change research. Quat. Sci. Rev. 355, 109233. https://doi.org/10.1016/j.quascirev.2025.109233.

Hadad, M.A., Santos, G.M., Roig Juñent, F.A., Grainger, C.S.G., 2015. Annual nature of the growth rings of *Araucaria araucana* confirmed by radiocarbon analysis. Quat. Geochronol. 30, 42–47. https://doi.org/10.1016/j.quageo.2015.05.002.

Harris, I., Osborn, T.J., Jones, P., Lister, D., 2020. Version 4 of the CRU TS monthly high-resolution gridded multivariate climate dataset. Scientific Data 7 (1), 109. https://doi.org/10.1038/s41597-020-04533.

He, L., Rodrigues, J.L.M., Mayes, M.A., Lai, C.T., Lipson, D.A., Xu, X., 2024. Modeling microbial carbon fluxes and stocks in global soils from 1901 to 2016. Biogeosciences 21 (9), 2313–2333. https://doi.org/10.5194/bg-21-2313-2024.

Hogg, A., Heaton, T.J., Hua, Q., Palmer, J.G., Turney, C.S.M., Southon, J., Bayliss, A., Blackwell, P.G., Boswijk, G., Bronk Ramsey, C., Pearson, C., Petchey, F., Reimer, P., Reimer, R., Wacker, L., 2020. SHCal20 southern hemisphere calibration, 0-55,000 years cal BP. Radiocarbon 62 (4), 759–778. https://doi.org/10.1017/RDC.2020.59.

Hua, Q., Barbetti, M., Jacobsen, G.E., Zoppi, U., Lawson, E.M., 2000. Bomb radiocarbon in annual tree rings from Thailand and Australia. Nucl. Instrum. Methods Phys. Res., Sect. B 172 (1–4), 359–365. https://doi.org/10.1016/S0168-583X(00)00147-6.

Hua, Q., Barbetti, M., Levchenko, V.A., D'Arrigo, R.D., Buckley, B.M., Smith, A.M., 2012. Monsoonal influences on Southern Hemisphere 14CO2. Geophys. Res. Lett. 39 (19), L19806. https://doi.org/10.1029/2012GL052971.

Hua, Q., Turnbull, J.C., Santos, G.M., Rakowski, A.Z., Ancapichún, S., De Pol-Holz, R., Hammer, S., Lehman, S.J., Levin, I., Miller, J.B., Palmer, J.G., 2022. Atmospheric radiocarbon for the period 1950–2019. Radiocarbon 64 (4), 723–745. https://doi.org/10.1017/RDC.2021.95.

Hubau, W., Lewis, S.L., Phillips, O.L., Affum-Baffoe, K., Beeckman, H., Cuní-Sanchez, A., Daniels, A.K., Ewango, C.E., Fauset, S., Mukinzi, J.M., Sheil, D., 2020. Asynchronous carbon sink saturation in African and Amazonian tropical forests. Nature 579 (7797), 80–87. https://doi.org/10.1038/s41586-020-2035-0.

Huntley, B.J., 2023. The Guineo-Congolian rain forest biome. In: Ecology of Angola: Terrestrial Biomes and Ecoregions. springer international publishing, Cham, pp. 279–304. https://doi.org/10.1007/978-3-031-18923-4_12 (ISBN 978-3-031-18923-4 (eBook)).

IPCC, 2023. Sections. In: Core Writing Team, Lee, H., Romero, J. (Eds.), Climate Change 2023: Synthesis Report. Contribution of Working Groups I, II and III to the Sixth Assessment Report of the Intergovernmental Panel on Climate Change. IPCC, Geneva, Switzerland, pp. 35–115. https://doi.org/10.59327/IPCC/AR6-9789291691647.

Kalnay, E., Kanamitsu, M., Kistler, R., Collins, W., Deaven, D., Gandin, L., Iredell, M., Saha, S., White, G., Woollen, J., Zhu, Y., Chelliah, M., Ebisuzaki, W., Higgins, W., Janowiak, J., Mo, K., Ropelewski, C., Wang, J., Leetmaa, A., Reynolds, R., Jenne, R., Joseph, D., 1996. The NCEP/NCAR 40-year reanalysis project. Bull. Am. Meteorol. Soc. 77, 437–471. https://doi.org/10.1175/1520-0477(1996)077<0437:TNYRP>2.0.CO;2.

Keeling, C.D., Piper, S.C., Bacastow, R.B., Wahlen, M., Whorf, T.P., Heimann, M., Meijer, H.A.J., 2001. Exchanges of atmospheric CO_2 and $^{13}CO_2$ with the terrestrial biosphere and oceans from 1978 to 2000. I. Global aspects, *SIO Reference Series, Scripps Institution of Oceanography,* San Diego, 88. https://escholarship.org/uc/item/09v319r9.

Kromer, B., Wacker, L., Friedrich, M., Lindauer, S., Friedrich, R., Bitterli, J., Treydte, K., Fonti, P., Martínez-Sancho, E., Nievergelt, D., 2024. Origin and age of carbon in the cellulose of mid-latitude tree rings. Radiocarbon 66. https://doi.org/10.1017/RDC.2024.38.

Kutschera, W., 2022. The versatile uses of the 14C bomb peak. Radiocarbon 64 (6), 1295–1308. https://doi.org/10.1017/RDC.2022.13.

Levin, I., Hesshaimer, V., 2000. Radiocarbon–a unique tracer of global carbon cycle dynamics. Radiocarbon 42, 69–80. https://doi.org/10.1017/S0033822200053066.

Levin, I., Kromer, B., 2004. The tropospheric 14CO2 level in mid-latitudes of the Northern Hemisphere (1959–2003). Radiocarbon 46 (3), 1261–1272. https://doi.org/10.1017/S0033822200033130.

Levin, I., Hammer, S., Kromer, B., Preunkert, S., Weller, R., Worthy, D.E., 2022. Radiocarbon in global tropospheric carbon dioxide. Radiocarbon 64 (4), 781–791. https://doi.org/10.1017/RDC.2021.102.

Linares, R., Santos, H.C., Brandes, A.F., Barros, C.F., Lisi, C.S., Balieiro, F.C., de Faria, S. M., 2017. Exploring the 14C bomb peak with tree rings of tropical species from the Amazon Forest. Radiocarbon 59 (2), 303–313. https://doi.org/10.1017/RDC.2017.10.

Longandjo, G.N.T., Rouault, M., 2024. Revisiting the seasonal cycle of rainfall over Central Africa. J. Climate 37 (3), 1015–1032. https://doi.org/10.1175/JCLI-D-23-0281.1.

Menne, M.J., Durre, I., Vose, R.S., Gleason, B.E., Houston, T.G., 2012. An overview of the global historical climatology network-daily database. J. Atmos. Oceanic Tech. 29 (7), 897–910. https://doi.org/10.1175/JTECH-D-11-00103.1.

Miner, K.R., Braghiere, R.K., Miller, C.E., Schlegel, N., Schimel, D., 2024. A decadal survey without analogs: earth observation needs for a warming world. AGU Adv. 5 (2), e2023AV001148. https://doi.org/10.1029/2023AV001148.

Muñoz, E., Chanca, I., Sierra, C.A., 2023. Increased atmospheric CO2 and the transit time of carbon in terrestrial ecosystems. Glob. Chang. Biol. 29 (23), 6441–6452. https://doi.org/10.1111/gcb.16961.

Murphy, J.O., Lawson, E.M., Fink, D., Hotchkis, M.A.C., Hua, Q., Jacobsen, G.E., Smith, A.M., Tuniz, C., 1997. 14C AMS measurements of the bomb pulse in N-and S-Hemisphere tropical trees. Nucl. Instrum. Methods Phys. Res., Sect. B 123 (1–4), 447–450. https://doi.org/10.1016/S0168-583X(96)00706-9.

Naegler, T., Levin, I., 2009. Biosphere-atmosphere gross carbon exchange flux and the δ13CO2 and Δ14CO2 disequilibria constrained by the biospheric excess radiocarbon inventory. J. Geophys. Res. 114, D17303. https://doi.org/10.1029/2008JD011116.

Nicholson, S.E., 2017. Evolving paradigms of climatic processes and atmospheric circulation affecting Africa. In: Oxford Research Encyclopedia of Climate Science. https://doi.org/10.1093/acrefore/9780190228620.013.515.

Nicholson, S.E., 2018. The ITCZ and the seasonal cycle over equatorial Africa. Bull. Am. Meteorol. Soc. 99 (2), 337–348. https://doi.org/10.1175/BAMS-D-16-0287.1.

Nicholson, S.E., Dezfuli, A.K., 2013. The relationship of rainfall variability in western equatorial Africa to the tropical oceans and atmospheric circulation. Part I: The boreal spring. J. Climate 26 (1), 45–65. https://doi.org/10.1175/JCLI-D-11-00653.1.

Nydal, R., Lövseth, K., 1983. Tracing bomb 14C in the atmosphere 1962–1980. J. Geophys. Res. Oceans 88 (C6), 3621–3642. https://doi.org/10.1029/JC088iC06p03621.

Olsson, I.U., 1980. 14C in extractives from wood. Radiocarbon 22 (2), 515–524. https://doi.org/10.1017/S0033822200009838.

Pan, Y., Birdsey, R.A., Phillips, O.L., Houghton, R.A., Fang, J., Kauppi, P.E., Keith, H., Kurz, W.A., Ito, A., Lewis, S.L., Nabuurs, G.J., 2024. The enduring world forest carbon sink. Nature 631 (8021), 563–569. https://doi.org/10.1038/s41586-024-07602-x.

Pereira, G.A., Barbosa, A.C.M.C., Torbenson, M.C.A., Stahle, D.W., Granato-Souza, D., Santos, R.M., Barbosa, J.P.D., 2018. The climate response of *Cedrela fissilis* annual ring width in the Rio São Francisco basin, Brazil. Tree-Ring Res. 74, 162–171. https://doi.org/10.3959/1536-1098-74.2.162.

Poorter, L., Bongers, F., Kouamé, F., 2004. Biodiversity of West African forests: an ecological atlas of woody plant species. CABI Publishing, Oxford, UK, p. 528 (pp. 0851997341). https://doi.org/10.1079/9780851997346.0041.

Poulter, B., Frank, D., Ciais, P., Myneni, R.B., Andela, N., Bi, J., Broquet, G., Canadell, J. G., Chevallier, F., Liu, Y.Y., Running, S.W., 2014. Contribution of semi-arid ecosystems to interannual variability of the global carbon cycle. Nature 509 (7502), 600–603. https://doi.org/10.1038/nature13376.

Randerson, J.T., Enting, I.G., Schuur, E.A.G., Caldeira, K., Fung, I.Y., 2002. Seasonal and latitudinal variability of troposphere Δ14CO2: post bomb contributions from fossil fuels, oceans, the stratosphere, and the terrestrial biosphere. Glob. Biogeochem. Cycles 16 (4). https://doi.org/10.1029/2002GB001876 (59-1).

Reimer, P.J., Austin, W.E., Bard, E., Bayliss, A., Blackwell, P.G., Bronk Ramsey, C., Butzin, M., Cheng, H., Edwards, R.L., Friedrich, M., Grootes, P.M., 2020. The IntCal20 Northern Hemisphere radiocarbon age calibration curve (0–55 cal kBP). Radiocarbon 62 (4), 725–757. https://doi.org/10.1017/RDC.2020.41.

Santos, G.M., Xu, X., 2017. Bag of tricks: a set of techniques and other resources to help 14C laboratory setup, sample processing, and beyond. Radiocarbon 59 (3), 785–801. https://doi.org/10.1017/RDC.2016.43.

Santos, G.M., Moore, R.B., Southon, J.R., Griffin, S., Hinger, E., Zhang, D., 2007. AMS 14C sample preparation at the KCCAMS/UCI Facility: status report and performance of small samples. Radiocarbon 49 (2), 255–269. https://doi.org/10.1017/S0033822200042181.

Santos, G.M., Linares, R., Lisi, C.S., Tomazello Filho, M., 2015. Annual growth rings in a sample of Paraná pine (*Araucaria angustifolia*): toward improving the 14C calibration curve for the southern hemisphere. Quat. Geochronol. 25, 96–103. https://doi.org/10.1016/j.quageo.2014.10.004.

Santos, G.M., Granato-Souza, D., Barbosa, A.C., Oelkers, R., Andreu-Hayles, L., 2020. Radiocarbon analysis confirms annual periodicity in Cedrela odorata tree rings from the equatorial Amazon. Quaternary Geochronology 58, 101079. https://doi.org/10.1016/j.quageo.2020.101079.

Santos, G.M., Rodriguez, D.R.O., Barreto, N.D.O., Assis-Pereira, G., Barbosa, A.C., Roig, F.A., Tomazello-Filho, M., 2021. Growth assessment of native tree species from the southwestern Brazilian Amazonia by post-AD 1950 14C analysis: implications for tropical dendroclimatology studies and atmospheric 14C reconstructions. Forests 12 (9), 1177. https://doi.org/10.3390/f12091177.

Santos, G.M., Albuquerque, R.P., Barros, C.F., Ancapichún, S., Oelkers, R., Andreu-Hayles, L., de Faria, S.M., De Pol-Holz, R., das Neves Brandes, A.F., 2022. High-precision ^{14}C measurements of parenchyma-rich *Hymenolobium petraeum* tree species confirm bomb-peak atmospheric levels and reveal local fossil-fuel CO_2 emissions in the central Amazon. Environ. Res. 214 (3), 113994. https://doi.org/10.1016/j.envres.2022.113994.

Santos, G.M., Komatsu, A.S., Renteria Jr., J.M., Brandes, A.F., Leong, C.A., Collado-Fabbri, S., De Pol-Holz, R., 2023. A universal approach to alpha-cellulose extraction for radiocarbon analysis of 14C-free to post-bomb ages. Quaternary Geochronology 74, 101414. https://doi.org/10.1016/j.quageo.2022.101414.

Santos, G.M., Granato-Souza, D., Ancapichún, S., Oelkers, R., Haines, H.A., De Pol-Holz, R., Andreu-Hayles, L., Hua, Q., Barbosa, A.C., 2024a. A novel post-1950 CE atmospheric 14C record for the tropics using absolutely dated tree rings in the equatorial Amazon. Sci. Total Environ. 918, 170686. https://doi.org/10.1016/j.scitotenv.2024.170686.

Santos, G.M., Nguyen, L.D., Griffin, J.N., Barreto, N.O., Ortega-Rodriguez, D.R., Barbosa, A.C., Assis-Pereira, G., 2024b. Evaluating possible sources of error in tree-ring 14C data using multiple trees across South America. Radiocarbon 67 (1), 1–16. https://doi.org/10.1017/RDC.2024.105.

Santos, G.M., Granato-Souza, D., Ancapichún, S., Oelkers, R., Haines, H.A., De Pol-Holz, R., Andreu-Hayles, L., Hua, Q., Barbosa, A.C., 2025. Data From: a Novel Post-1950 CE Atmospheric 14C Record for the Tropics Using Absolutely Dated Tree Rings in the Equatorial Amazon [dataset]. Dryad. https://doi.org/10.5061/dryad.xsj3tx9rd.

Scott, E.M., Boaretto, E., Bryant, C., Cook, G.T., Gulliksen, S., Harkness, D.D., Heinemeier, J., McGee, E., Naysmith, P., Possnert, G., van der Plicht, H., 2004. Future needs and requirements for AMS 14C standards and reference materials. Nucl. Instrum. Methods Phys. Res. Sect. B Beam Interact. Mater. Atoms 223, 382–387. https://doi.org/10.1016/j.nimb.2004.04.074.

Shi, Z., Allison, S.D., He, Y., Levine, P.A., Hoyt, A.M., Beem-Miller, J., Zhu, Q., Wieder, W.R., Trumbore, S., Randerson, J.T., 2020. The age distribution of global soil carbon inferred from radiocarbon measurements. Nat. Geosci. 13 (8), 555–559. https://doi.org/10.1038/s41561-020-0596-z.

Staal, A., van Nes, E.H., Hantson, S., Holmgren, M., Dekker, S.C., Pueyo, S., Xu, C., Scheffer, M., 2018. Resilience of tropical tree cover: the roles of climate, fire, and herbivory. Glob. Chang. Biol. 24 (11), 5096–5109. https://doi.org/10.1111/gcb.14408.

Stein, A., Draxler, R., Rolph, G., Stunder, B., Cohen, M., Ngan, F., 2015. NOAA's HYSPLIT atmospheric transport and dispersion modeling system. Bull. Am. Meteorol. Soc. 96, 2059–2077. https://doi.org/10.1175/BAMS-D-14-00110.1.

Stuiver, M., Polach, H.A., 1977. Discussion: reporting of 14C data. Radiocarbon 19, 355–363. https://doi.org/10.1017/S0033822200003672.

Suess, H.E., 1955. Radiocarbon concentration in modern wood. Science 122 (3166), 415–417. https://doi.org/10.1126/science.122.3166.415.

Tamoffo, A.T., Weber, T., Cabos, W., Monerie, P.A., Cook, K.H., Sein, D.V., Dosio, A., Klutse, N.A., Akinsanola, A.A., Jacob, D., 2024. West African monsoon system's responses to global ocean-regional atmosphere coupling. J. Climate 37 (16), 4291–4312. https://doi.org/10.1175/JCLI-D-23-0749.1.

Tandoh, J.B., Marzaioli, F., Battipaglia, G., Capano, M., Castaldi, S., Lasserre, B., Marchetti, M., Passariello, I., Terrasi, F., Valentini, R., 2013. Biomass growth rate of trees from Cameroon based on 14C analysis and growth models. Radiocarbon 55 (2), 885–893. https://doi.org/10.1017/S0033822200058045.

Tchiofo-Lontsi, R., Corre, M.D., Iddris, N.A., Veldkamp, E., 2020. Soil greenhouse gas fluxes following conventional selective and reduced-impact logging in a Congo Basin rainforest. Biogeochemistry 151 (2–3), 153–170. https://doi.org/10.1007/s10533-020-00718-y.

Tegegne, Y.T., Lindner, M., Fobissie, K., Kanninen, M., 2016. Evolution of drivers of deforestation and forest degradation in the Congo Basin forests: exploring possible policy options to address forest loss. Land Use Policy 51, 312–324. https://doi.org/10.1016/j.landusepol.2015.11.024.

Thorncroft, C.D., Nguyen, H., Zhang, C., Peyrillé, P., 2011. Annual cycle of the west African monsoon: regional circulations and associated water vapour transport. Q. J. Roy. Meteorol. Soc. 137 (654), 129–147. https://doi.org/10.1002/qj.728.

Toggweiler, J.R., Druffel, E.R., Key, R.M., Galbraith, E.D., 2019. Upwelling in the ocean basins north of the ACC: 1. On the upwelling exposed by the surface distribution of Δ14C. J. Geophys. Res. Oceans 124 (4), 2591–2608. https://doi.org/10.1029/2018JC014795.

TRC, 2006. La Société Transformation Reef Cameroun, Convention Provisoire d'Exploitation, – Plan d'aménagement Concession N°1086 UFA 11-001. In. Ets MEDINOF, Douala – Cameroon. URL. https://www.openlandcontracts.org/contract/ocds-591adf-6717687046/view#/pdf.

van der Sleen, P., Groenendijk, P., Zuidema, P.A., 2015. Tree-ring δ18O in African mahogany (Entandrophragma utile) records regional precipitation and can be used for climate reconstructions. Global Planet. Change 127, 58–66. https://doi.org/10.1016/j.gloplacha.2015.01.014.

Varga, T., Orsovszki, G., Major, I., Veres, M., Bujtás, T., Végh, G., Manga, L., Jull, A.T., Palcsu, L., Molnár, M., 2020. Advanced atmospheric ^{14}C monitoring around the Paks nuclear power plant, Hungary. J. Environ. Radioact. 213, 106138. https://doi.org/10.1016/j.jenvrad.2019.106138.

Verhegghen, A., Eva, H., Desclée, B., Achard, F., 2016. Review and combination of recent remote sensing based products for forest cover change assessments in Cameroon. Int. For. Rev. 18 (1), 14–25. https://doi.org/10.1505/146554816819683807.

Villarreal, S., Vargas, R., 2021. Representativeness of FLUXNET sites across Latin America. J. Geophys. Res. Biogeosciences 126 (3), e2020JG006090. https://doi.org/10.1029/2020JG006090.

Vondou, D.A., 2012. Spatio-temporal variability of Western Central African convection from infrared observations. Atmosphere 3 (3), 377–399. https://doi.org/10.3390/atmos3030377.

Wang, X., Piao, S., Ciais, P., Friedlingstein, P., Myneni, R.B., Cox, P., Heimann, M., Miller, J., Peng, S., Wang, T., Yang, H., 2014. A two-fold increase of carbon cycle sensitivity to tropical temperature variations. Nature 506 (7487), 212–215. https://doi.org/10.1038/nature12915.

Wiggins, E.B., Czimczik, C.I., Santos, G.M., Chen, Y., Xu, X., Holden, S.R., Randerson, J. T., Harvey, C.F., Kai, F.M., Yu, L.E., 2018. Smoke radiocarbon measurements from Indonesian fires provide evidence for burning of millennia-aged peat. Proc. Natl. Acad. Sci. 115 (49), 12419–12424. https://doi.org/10.1073/pnas.1806003115.

Worbes, M., 2002. One hundred years of tree-ring research in the tropics–a brief history and an outlook to future challenges. Dendrochronologia 20 (1–2), 217–231. https://doi.org/10.1078/1125-7865-00018.

Xu, X., van der Sleen, P., Groenendijk, P., Vlam, M., Medvigy, D., Moorcroft, P., Petticord, D., Ma, Y., Zuidema, P.A., 2024. Constraining long-term model predictions for woody growth using tropical tree rings. Glob. Chang. Biol. 30 (1), e17075. https://doi.org/10.1111/gcb.17075.

Yakusu, E.K., Monthe, F.S., Bourland, N., Hardy, O.J., Louppe, D., Lokanda, F.B.M., Hubau, W., Muhongya, J.-M.K., Bulcke, J.V.D., Acker, J.V., Beeckman, H., 2018.

Entandrophragma: taxonomy and ecology of a genus of African tree species with economic importance. A review. Biotechnol. Agron. Soc. Environ. 22 (2), 113–127. https://doi.org/10.25518/1780-4507.19073.

Zhao, S., Pederson, N., D'Orangeville, L., HilleRisLambers, J., Boose, E., Penone, C., Bauer, B., Jiang, Y., Manzanedo, R.D., 2019. The International Tree-Ring Data Bank (ITRDB) revisited: data availability and global ecological representativity. J. Biogeogr. 46 (2), 355–368. https://doi.org/10.1111/jbi.13488.

Zhao, Z., Ding, X., Wang, G., Li, Y., 2024. 30 m resolution global maps of forest soil respiration and its changes from 2000 to 2020. Earths Future 12 (2), e2023EF004007. https://doi.org/10.1029/2023EF004007.

Zubkova, M., Boschetti, L., Abatzoglou, J.T., Giglio, L., 2019. Changes in fire activity in Africa from 2002 to 2016 and their potential drivers. Geophys. Res. Lett. 46 (13), 7643–7653. https://doi.org/10.1029/2019GL083469.